THE INCLUSION OF MOISTURE IN A NUMERICAL MODEL OF STEADY-STATE FRONTS

Clifford James Cornelius

NAVAL POSTGRADUATE SCHOOL
Monterey, California

THESIS

THE INCLUSION OF MOISTURE IN A NUMERICAL MODEL OF STEADY-STATE FRONTS

by

Clifford James Cornelius, Jr.

Thesis Advisor: R. T. Williams

March 1974

The Inclusion of Moisture in a Numerical Model of Steady-State Fronts

by

Clifford James Cornelius, Jr.
Lieutenant, United States Navy
B.S. in ED., Seton Hall University, 1964

Submitted in partial fulfillment of the
requirements for the degree of

MASTER OF SCIENCE IN METEOROLOGY

from the

NAVAL POSTGRADUATE SCHOOL
March 1974

ABSTRACT

The numerical frontogenesis model of Williams (1973) is modified to include moisture with its subsequent condensation and release of latent heating. The turbulent diffusions of momentum, heat and moisture are represented with various coefficients. The numerical solutions show realistic quasi-steady fronts forming within one to two days. These solutions are examined and compared over a range of the various coefficients, and various ranges of temperature.

Inclusion of moisture in the model causes intensification of baroclinicity at mid and upper levels. Also noted is a sensitivity of the moist model to reference potential temperature due to the exponential relationship between saturation vapor pressure and temperature.

TABLE OF CONTENTS

LIST OF TABLES

LIST OF ILLUSTRATIONS

ACKNOWLEDGEMENTS

The author wishes to express his appreciation to Dr. Roger Terry Williams for his technical assistance, recommendations, encouragement, and for the use of his steady-state frontogenesis model which was modified for the experiments conducted.

Thanks are expressed to Dr. Robert L. Haney, who acted as second reader, for his constructive comments on the manuscript.

Thanks are also expressed to Dr. George J. Haltiner who provided information on schemes for dry and moist convective adjustment and to William Ehrman of the W. R. Church Computer Center who unselfishly gave of his time to help in improving the author's programming efficiency.

The author furthermore wishes to acknowledge the W. R. Church Computer Center at the Naval Postgraduate School on whose computer system IBM 360/67 all computations were performed.

A final acknowledgement is given to Charlotte S. Cornelius who now awaits the author's return after a long absence.

I. INTRODUCTION

Hoskins and Bretherton (1972) have shown analytically, and Williams (1967, 1972) has shown numerically that discontinuous fronts can form within a finite period of time if no turbulent diffusion is present. These studies suggest that a discontinuity will form within 24 to 36 hours when reasonable initial conditions are used. If turbulent diffusion is present, it can be expected that a balance will be achieved between the frontogenetic advections and turbulent diffusions of momentum, heat, and moisture. The front should remain in this state of quasi-balance as long as the large scale deformation field causes frontogenetic advections around the front.

The numerical frontogenesis model of Williams (1973) shows the effects of horizontal and vertical turbulent diffusions of momentum and heat in the formation of these quasi-steady fronts. This model, which also includes an Ekman boundary layer, will hereafter be referred to as W73 and the model as it existed in Williams (1972) will be referred to as W72.

This investigation appends moisture with its subsequent condensation and release of latent heating to W73. It is assumed that all the latent heat released in this condensation is used to heat the air isobarically.

The purpose of this study is to obtain and examine frontal solutions from the model throughout a four day period. The physical model is essentially the same as one of the models treated by Hoskins (1971) and Hoskins and Bretherton (1972). The basic model, as it now exists, numerically describes frontogenesis which is forced by a nondivergent horizontal wind field which contains stretching deformation. This deformation wind field is constant in time and is independent of height, except in the Ekman boundary layer. The moist hydrostatic primitive equations with diffusion are used in which the time dependent quantities are functions of Y and P only. Therefore, output from the model is in the form of vertical cross-sections in the Y-P plane.

W73 has been transformed to pressure coordinates to obtain more accurate values of pressure for the moisture equations that have been included in the present model.

In Section 2, the basic forecast equations are developed, transformed to pressure coordinates and a simplification which keeps the problem two dimensional is discussed. The initial conditions are presented and transformed to pressure coordinates in Section 3. Convective adjustment processes and latent heat release in the model are included in Section 4. The experiments undertaken are examined in Section 5 and conclusions are given in Section 6.

II. BASIC EQUATIONS AND BOUNDARY CONDITIONS

The hydrostatic primitive equations with diffusion and moisture may be written as follows:

$$\frac{\partial \underset{\sim}{V}}{\partial t} + \nabla\cdot(\underset{\sim\sim}{VV}) + \frac{\partial(w\underset{\sim}{V})}{\partial s} + \nabla\phi + f(\kappa x \underset{\sim}{V}) = A_m\nabla^2\underset{\sim}{V} + C_m\frac{\partial^2\underset{\sim}{V}}{\partial s^2}\ , \qquad (2.1)$$

$$\frac{\partial\theta}{\partial t} + \nabla\cdot(\theta\underset{\sim}{V}) + \frac{\partial}{\partial s}(w\theta) = A_\theta\nabla^2\theta + C_\theta\frac{\partial^2\theta}{\partial s^2} + Q_A + Q_M + H_C\ , \qquad (2.2)$$

$$\frac{\partial q}{\partial t} + \nabla\cdot(q\underset{\sim}{V}) + \frac{\partial}{\partial s}(wq) = A_q\nabla^2 q + C_q\frac{\partial^2 q}{\partial s^2} + M_A - M_C\ , \qquad (2.3)$$

$$\nabla\cdot\underset{\sim}{V} + \frac{\partial w}{\partial s} = 0\ , \qquad (2.4)$$

$$\frac{\partial\phi}{\partial s} = L(s)\theta\ , \qquad (2.5)$$

where the vertical coordinate has been replaced by s to aid in later discussions on transformation. The equations are from W73 with slight modification due to the addition of the equation of conservation of water wapor (2.3) which is analogous to the thermodynamic equation (2.2). The function L(s) in the hydrostatic equation (2.5) is a constant g/θ_o in height coordinates. Also sinks and sources of heating and moisture have been added to the thermodynamic equation (2.2) and the conservation of water vapor equation (2.3).

The notation used is basically the same as W72 which uses height as the vertical coordinate. However, in our

subsequent transformation to pressure coordinates, θ is defined as a departure from the domain average of the initial state, ϕ represents geopotential, gz and w is ds/dt in the continuity equation (2.4), thereby allowing compressibility.

The quantities, A_m, A_θ, and A_q are the horizontal turbulent diffusion coefficients of momentum, heat, and moisture, respectively, while C_m, C_θ, and C_q are the corresponding vertical coefficients. These constant coefficients were assigned various reasonable values in the different moisture experiments. Dry and moist convective adjustment processes are represented by the functions Q_A and Q_M while latent heating due to large scale condensation is represented by H_C. In the moisture equation, M_A is a sink or source of moisture due to moist convective adjustment while M_C is a sink for moisture due to large scale condensation.

Boundary conditions for the above equations are such that the domain is bounded by two rigid quasi-horizontal planes. The no-slip condition at the lower boundary and the no-stress condition at the top roughly represents the troposphere. The conditions are as follows:

$$\left.\begin{aligned} & w(x,y,o,t) = w(x,y,H,t) = 0 \\ & \underset{\sim}{V}(x,y,o,t) = 0 \\ & C_m \frac{\partial \underset{\sim}{V}}{\partial s}(x,y,H,t) = 0 \\ & C_\theta \frac{\partial \theta}{\partial s}(x,y,o,t) = C_\theta \frac{\partial \theta}{\partial s}(x,y,H,t) = 0 \\ & C_q \frac{\partial q}{\partial s}(x,y,o,t) = C_q \frac{\partial q}{\partial s}(x,y,H,t) = 0 \end{aligned}\right\}, \quad (2.6)$$

where H represents the distance between the upper and lower boundaries. The lower boundary conditions are realistic for fronts over level terrain. Therefore, frontogenesis in the lower troposphere is more realistic in the model than are conditions near the "tropopause". The additional boundary conditions for moisture are completely analogous to the heating conditions in that fluxes of the quantities do not pass through the boundaries.

The approximate steady state solutions to the hydrostatic primitive equations from [(2.1)-(2.5)] are:

$$\left.\begin{aligned} \underset{\sim}{V} = \underset{\sim}{U} &\equiv D\{[x(1-e^{-Bs}\cos Bs) + ye^{-Bs}\sin Bs]\ \underset{\sim}{i} \\ &- [y(1-e^{-Bs}\cos Bs) - xe^{-Bs}\sin Bs]\ \underset{\sim}{j}\} \\ w &= 0\ , \\ \phi = \Phi &\equiv -D^2(x^2 + y^2)/2 - fD\,xy + F(s) \\ \theta &= G(s) \\ q &= H(s) \end{aligned}\right\}\ , \qquad (2.7)$$

where $B = (f/2C_m)^{1/2}$, D and f are constant and where F(s) is such that the hydrostatic equation (2.5) is satisfied. The functions G(s) and H(s) are arbitrary functions of s since w = 0. These solutions satisfy the boundary conditions (2.6) and allow for inclusion of the Ekman boundary layer. These relations (2.7) satisfy the steady-state equations if some small advection terms in the boundary layer are neglected. These small terms are usually dropped in the Ekman Theory.

The equations and the model become two dimensional after a subdivision of the dependent variables as follows:

$$\left.\begin{aligned} \underset{\sim}{V} &= \underset{\sim}{U}(x,y,x) + u(y,s,t)\underset{\sim}{i} + v(y,s,t)\underset{\sim}{j} \\ w &= w(y,s,t) \\ \theta &= \theta(y,s,t) \\ \phi &= \Phi(x,y) + \pi(y,s,t) \\ q &= q(y,s,t) \end{aligned}\right\} . \qquad (2.8)$$

It is noted that all departures from the approximate steady deformation solutions (2.7) are assumed to be independent of x. If we substitute the relations (2.8) in the $\underset{\sim}{i}$ component of (2.1) we obtain:

$$\frac{\partial u}{\partial t} + \frac{\partial}{\partial y}(uv) + \frac{\partial}{\partial s}(wu) + uD(1-e^{-Bs}\cos Bs)$$
$$-D[y(1-e^{-Bs}\cos Bs)-xe^{-Bs}\sin Bs]\frac{\partial u}{\partial y} + vDe^{-Bs}\sin Bs$$
$$+wD\frac{\partial}{\partial s}[xe^{-Bs}(1-\cos Bs)+ye^{-Bs}\sin Bs]=fv+A_m\frac{\partial^2 u}{\partial y^2}$$
$$+ C_m\frac{\partial^2 u}{\partial s^2} . \qquad (2.9)$$

Note that the assumption that u is independent of x for all time is violated in (2.9) in the two terms where x appears. This indicates that the other quantities which were assumed independent of x are, in fact, x-dependent and this would bring other terms into the equations. In this study we will neglect these added terms and apply (2.9) and the other equations at x = 0. If the initial u,v,w,θ,π and q fields are independent of x, the

error from this approximation will grow slowly and will be confined to the boundary layer since the x-dependent terms in (2.9) are zero outside the boundary layer. Since frontogenesis occurs very rapidly it is expected that the development of x-variations in the dependent variables would have only a small effect on the resulting quasi-steady front. In any case these effects could not be observed in the atmosphere, because atmospheric fronts have some variation in the basic fields along the front which would be much more important.

When equation (2.9) is evaluated at x = 0 it becomes

$$\frac{\partial u}{\partial t} + \frac{\partial (uv)}{\partial y} + \frac{\partial (wu)}{\partial s} - \Gamma u \frac{\partial V}{\partial y} + \Gamma V \frac{\partial u}{\partial y} - \frac{v \partial V}{\partial y}(e^{-Bs} \sin Bs)$$

$$-Vw \frac{\partial}{\partial s}(e^{-Bs} \sin Bs) = fv + A_m \frac{\partial^2 u}{\partial y^2} + C_m \frac{\partial^2 u}{\partial s^2} , \qquad (2.10)$$

where $V = -Dy$ and $\Gamma = 1 - e^{Bs} \cos Bs$. The $\underset{\sim}{j}$ component of (2.1) applied at x = 0 takes the form

$$\frac{\partial v}{\partial t} + \frac{\partial}{\partial y}(vv) + \frac{\partial}{\partial s}(wv) + \Gamma \frac{\partial}{\partial y}(vV) - u \frac{\partial V}{\partial y} e^{-Bs} \sin Bs$$

$$-(wV)\frac{\partial}{\partial s}(e^{-B} \cos B) = -\frac{\partial \pi}{\partial y} - fu + A_m \frac{\partial^2 u}{\partial y^2} + C_m \frac{\partial^2 v}{\partial s^2} . \qquad (2.11)$$

In a similar manner from equation (2.2), the following equation for the departure of potential temperature can be derived:

$$\frac{\partial \theta}{\partial t} + \frac{\partial (v\theta)}{\partial y} + \frac{\partial (w\theta)}{\partial s} + \Gamma V \frac{\partial \theta}{\partial y} = A_\theta \frac{\partial^2 \theta}{\partial y^2} + C_\theta \frac{\partial^2 \theta}{\partial s^2}$$

$$+ Q_a + Q_m + H_c , \qquad (2.12)$$

and the following equation for q follows from (2.3),

$$\frac{\partial q}{\partial t} + \frac{\partial (vq)}{\partial y} + \frac{\partial}{\partial s}(wq) + \Gamma v \frac{\partial q}{\partial y} = A_q \frac{\partial^2 q}{\partial y^2} + C_q \frac{\partial^2 q}{\partial s^2}$$

$$+ M_A - M_C \ , \qquad (2.13)$$

Equations (2.4) and (2.5) become

$$\frac{\partial v}{\partial y} + \frac{\partial w}{\partial s} = 0 \ , \qquad (2.14)$$

and

$$\frac{\partial \pi}{\partial s} = L(s)\ \theta \ . \qquad (2.15)$$

The boundary conditions at the bottom and top of the domain respectively are

$$\left.\begin{aligned} u = v = w = C_\theta \frac{\partial \theta}{\partial s} = C_q \frac{\partial q}{\partial s} = 0 \ , \ s = 0 \\ C_m \frac{\partial u}{\partial s} = C_m \frac{\partial v}{\partial s} = w = C_\theta \frac{\partial \theta}{\partial s} = C_q \frac{\partial q}{\partial s} = 0 \ , \ s = H \end{aligned}\right\} . \qquad (2.16)$$

If we define the vertical average of a quantity as

$$< \ (\ ) \ > = \frac{1}{H} \int_o^H (\ ) \ ds \ , \qquad (2.17)$$

integrate the hydrostatic equation (2.15) with respect to s, and remove the vertical mean, it follows that

$$\pi - <\pi> = \left[\int_o^s L(s)\theta ds - < \int_o^s L(s)\theta ds > \right] . \qquad (2.18)$$

Take the vertical average of (2.14) and use the boundary (2.16) which gives

$$\frac{\partial}{\partial y} <v> = 0 \ . \qquad (2.19)$$

This equation states that the total mass flux in the $\tilde{j}$ direction is independent of y. In W72 a symmetry argument was used to show that this flux must be zero. This argument does not hold strictly in the present experiment, but it can be expected that at large distances from the frontal zone the disturbance mass flux will vanish. Thus, it is assumed that

$$< v > = 0 \, . \tag{2.20}$$

If the development of W72 is used, equation (2.11) can be written

$$\frac{\partial v}{\partial t} + \frac{\partial}{\partial y}[vv - <vv>] + \frac{\partial}{\partial s}(wv) + \frac{\partial}{\partial y}(\Gamma v V - <\Gamma v> V)$$

$$- \frac{\partial V}{\partial y}[ue^{-Bs}\sin Bs - <ue^{-Bs}\sin Bs> - V[w \frac{\partial}{\partial s}(e^{-Bs}\cos Bs)$$

$$- <w \frac{\partial}{\partial s}(e^{-Bs}\cos Bs)>] = - \frac{\partial}{\partial y}(\pi - <\pi>) - f(u - <u>)$$

$$+ A_m \frac{\partial^2 v}{\partial y^2} + C_m[\frac{\partial^2 v}{\partial s^2} + \frac{1}{H}(\frac{\partial v}{\partial s})_{s=0}] \, . \tag{2.21}$$

The equations (2.10), (2.12), (2.13), (2.14), (2.18) and (2.21) form a complete set which can be solved by a pure marching process. The finite difference equations conserve mean squares in the advection terms and are described by Williams (1967). The Matsuno scheme is used everywhere except in the arrangement of variables and the finite difference approximations are the same as those used by Williams (1967). In order to close the problem,

computational boundaries must be introduced in y. Since the disturbance velocities should die out at a sufficient distance from the axis of dilation, then

$$v(\pm Y,s,t) = 0 \ . \qquad (2.22)$$

However, there is appreciable inflow across these computational boundaries since $V(\pm Y) = \pm DY$. The quantities u, θ, and q which are advected across the boundaries must be specified independent of the interior values if computational stability is to be maintained (Platzman, 1954). Thus, the following boundary conditions are used:

$$\left.\begin{aligned} u[\pm(Y + \Delta y/2),s,t] &= u\ [\pm(Y + \Delta y/2),s,0] \\ \theta[\pm(Y + \Delta y/2),s,t] &= \theta\ [\pm(Y + \Delta y/2),s,0] \\ q[\pm(Y + \Delta y/2),s,t] &= q\ [\pm(Y + \Delta y/2),s,0] \end{aligned}\right\} \ . \qquad (2.23)$$

The computational boundaries $y = \pm Y$ are placed between gridpoints so that the above conditions are actually applied at $y \neq \pm (Y + \Delta y/2)$.

The boundary conditions were found to be satisfactory except that a solution separation developed near the boundaries. This was controlled by using a Matsuno time differencing scheme for stability.

In order to have precise values of pressure at gridpoints for the moisture experiments it was deemed necessary to transform W72 to pressure coordinates. Minimization of changes to finite differencing schemes

of the model have been achieved by defining a parameter s which is analogous to a field of z. Specifically,

$$s = P_o - P \ , \tag{2.24}$$

a field that will increase in the upward direction and from which values of pressure can easily be obtained. Further, it is seen that $\partial s = - \partial P$ so that finite differencing schemes in W72 can be equally well applied to the field s.

Through the expression in s coordinates the momentum equations (2.10) and (2.21), the thermodynamic equation (2.12) and the moisture equation (2.13) remain as before for the model. However, the continuity equation (2.14) in the model actually remains in w and describes a negative field of omega in that,

$$w \equiv \frac{ds}{dt} = -\omega \ . \tag{2.25}$$

Equation (2.5), the hydrostatic equation, differs significantly due to the transformation. The derivation is briefly as follows. The hydrostatic equation expressed in pressure coordinates and the equation of state gives

$$\frac{\partial \phi}{\partial p} = -\alpha = - \frac{RT}{p} \ . \tag{2.26}$$

If a form of the potential temperature definition is used,

$$T = \theta \left(\frac{p}{p_o}\right)^{\kappa} \ , \tag{2.27}$$

and combined with (2.26) and (2.27) it follows

$$\frac{\partial \phi}{\partial p} = - \frac{R}{p} \left(\frac{p}{p_o}\right)^{\kappa} \theta \ . \qquad (2.28)$$

It can be shown that

$$\frac{R}{p} \left(\frac{p}{p_o}\right)^{\kappa} = C_p \frac{\partial}{\partial p} \left(\frac{p}{p_o}\right)^{\kappa} \ . \qquad (2.29)$$

The latter form simplifies finite difference energy conservation. Therefore, substituting equation (2.29) into equation (2.28) and transforming to s coordinates we obtain

$$\frac{\partial \phi}{\partial s} = - C_p \frac{\partial}{\partial s} \left[\left(\frac{p}{p_o}\right)^{\kappa}\right] \theta \ , \qquad (2.30)$$

a form of the hydrostatic equation. Note that L(s) is not constant as in height coordinates since

$$L(s) = \frac{R}{p} \left(\frac{p}{p_o}\right)^{\kappa} = - C_p \frac{\partial}{\partial s} \left(\frac{p}{p_o}\right)^{\kappa} \ . \qquad (2.31)$$

It follows that the complete set of equations solved by the marching process remains intact but with L(s) defined as in (2.31).

The boundary conditions (2.16) also remain intact except that the lower boundary of vertical motion in the model is approximated as

$$w = - \omega = 0 \ , \text{ at } s = 0 \ . \qquad (2.32)$$

III. INITIAL CONDITIONS

The initial conditions in height of s coordinates are the same as those employed in W73. The initial potential temperature field is given by

$$\theta(y,z,o) = [\frac{\partial \overline{\theta}_I}{\partial z} (z - \frac{H}{2})] - a(\frac{2}{\pi}) \arctan (\sinh \alpha y)$$

where

$$\alpha = \frac{f\pi}{H\sqrt{L(s) \frac{\partial \overline{\theta}_I}{\partial z}}} . \qquad (3.1)$$

The quantity $\partial \overline{\theta}_I / \partial z$ which is constant is the initial static stability, $\overline{\theta}_I$ being the initial horizontally averaged initial theta and "a" is one-half the total horizontal temperature variation.

By substituting equation (3.1) into the thermal wind equation and integrating we obtain the x-component of the rotational wind which is

$$u(y,z,o) = \frac{2}{\pi} \frac{ga\alpha}{f\theta_o} (z - \frac{H}{2}) \operatorname{sech} \alpha y . \qquad (3.2)$$

The divergent part of the wind or v field is obtained from the quasi-geostrophic equations in z coordinates. Details are as in Williams (1972). The remaining fields of w and π are obtained from the continuity (2.14) and hydrostatic (2.15) equations.

Once again transformation of the above initial fields must be made to pressure coordinates.

To obtain initial conditions for the theta field we must first find $\overline{\Theta}_I$, the horizontally averaged initial theta based on $\Theta_I(p_o)$. Derivation is as follows. Given knowledge of differentials and the definition of geopotential it is seen that

$$\frac{\partial \overline{\Theta}_I}{\partial p} = \frac{\partial \overline{\Theta}_I}{\partial z} \frac{\partial z}{\partial p} = \frac{1}{g} \frac{\partial \theta_I}{\partial z} \frac{\partial \phi}{\partial p} , \tag{3.3}$$

where $\partial \overline{\Theta}_I / \partial z$ is the prescribed static stability at $t = 0$.

Substitute a definition of potential temperature (2.27) to obtain

$$\frac{\partial \overline{\Theta}_I}{\partial p} = \frac{\partial \overline{\Theta}_I}{\partial z} \left[- \frac{1}{g} \frac{R}{p} \left(\frac{p}{p_o}\right)^{\kappa} \right] \overline{\Theta}_I . \tag{3.4}$$

Integrate from p_o to some p ,

$$\int_{p_o}^{p} \frac{1}{\overline{\Theta}_I} \frac{\partial \overline{\Theta}_I}{\partial p} \, dp = \int_{p_o}^{p} - \frac{R}{g} \frac{\partial \overline{\Theta}_I}{\partial z} \frac{1}{p} \left(\frac{p}{p_o}\right)^{\kappa} dp , \tag{3.5}$$

which yields

$$\ln \frac{\overline{\Theta}_I}{\overline{\Theta}_I(p_o)} = - \frac{R}{g} \frac{\partial \overline{\Theta}_I}{\partial z} \kappa \left[\left(\frac{p}{p_o}\right)^{\kappa} - \left(\frac{p_o}{p_o}\right)^{\kappa} \right] . \tag{3.6}$$

where $\kappa = R/C_p$, it follows that

$$\overline{\Theta}_I(p) = \overline{\Theta}_I(p_o) \, \mathrm{EXP}\left[\frac{C_p}{g} \frac{\partial \overline{\Theta}_I}{\partial z} \left(1 - \left(\frac{p}{p_o}\right)^{\kappa}\right) \right] . \tag{3.7}$$

Equation (3.7) is representative of term one of equation (3.1). Therefore, the initial potential temperature field in pressure coordinates is given by

$$\Theta_I(y,p,o) = \overline{\Theta}_I(p_o)\ \mathrm{EXP}\left[\frac{c_p}{g}\frac{\partial\overline{\Theta}_I}{\partial z}\left(1-\left(\frac{p}{p_o}\right)^{\kappa}\right)\right]$$

$$-a(2/\pi)\ \arctan\ (\sinh\ \alpha\ y)\ . \qquad (3.8)$$

where

$$\alpha \approx \frac{f\pi}{H\sqrt{L(s_m)\left(-\frac{\partial\overline{\Theta}_I}{\partial p}\right)}} \approx \frac{f\pi}{H\sqrt{\frac{R}{p_m}\left(\frac{p_m}{p_o}\right)^{\kappa}\left(-\frac{\partial\overline{\Theta}_I}{\partial p}\right)_m}} \qquad (3.9)$$

In the model α is given a constant median value by solving equation (3.10) at $p = p_m = 60$ cb and using the static stability $\partial\Theta_I/\partial p$ at this level. Recall also that pressure in equation (3.8) can easily be obtained for model purposes as $p = p_o - s$.

Further it should be recalled that θ is a departure from the domain average of Θ_I. This domain average is found in the model by finding the vertical average of equation (3.7), $\langle \overline{\Theta}_I \rangle$.

The initial x-component of the velocity or initial u equation is found using a form of the hydrostatic equation (2.26) and the definition of geostrophic wind,

$$u = -\frac{1}{f}\frac{\partial\phi}{\partial y}\ , \qquad (3.10)$$

A form of the thermal wind equation is found to be

$$\frac{\partial u}{\partial p} = -\frac{1}{f}\frac{\partial}{\partial y}\frac{\partial\phi}{\partial p} = +\frac{1}{f}\frac{R}{p}\left(\frac{p}{p_o}\right)^{\kappa}\frac{\partial\theta}{\partial y}\ . \qquad (3.11)$$

If we again assume a median pressure level p_m = 60 cb, and that at this level $u(p_m) = 0$, we integrate

$$\int_{p_m}^{p} \frac{\partial u}{\partial p}\, dp = \frac{R}{f} \frac{\partial \theta}{\partial y} \int_{p_m}^{p} \frac{1}{p}\left(\frac{p}{p_o}\right)^{\kappa} dp \ . \qquad (3.12)$$

Recalling that $u(p_m) = 0$ and that $\kappa = R/C_p$ the integration yields

$$u(y,p,o) = \frac{C_p}{f} \frac{\partial \theta}{\partial y} \left[\left(\frac{p}{p_o}\right)^{\kappa} - \left(\frac{p_m}{p_o}\right)^{\kappa}\right] \ . \qquad (3.13)$$

From (Williams, 1972) equation (4.3), it is seen that

$$\frac{\partial \theta}{\partial y} = - \frac{2a\alpha}{\pi} \operatorname{sech}(\alpha y) \ . \qquad (3.14)$$

Therefore, the initial u field in pressure coordinates is given by

$$u(y,p,o) = -\frac{C_p}{f} \frac{2a\alpha}{\pi} \left[\left(\frac{p}{p_o}\right)^{\kappa} - \left(\frac{p_m}{p_o}\right)^{\kappa}\right] \operatorname{sech}(\alpha y) \ . \qquad (3.15)$$

The initial divergent wind v is determined as in Williams (1972) but using the quasi-geostrophic equation in pressure coordinates. The stream function is defined as

$$\left.\begin{aligned} v &= \partial\Psi/\partial p \\ \text{and} \quad \omega &= -\partial\psi/\partial y \end{aligned}\right\}, \qquad (3.16)$$

and equation (4.10) of Williams (1972) takes the form

$$-\frac{\partial^2 \psi}{\partial p^2} + L(s_m)\left(-\frac{\partial \theta}{\partial p}_I\right)_{p_m} \frac{\partial^2 \psi}{\partial y^2} = \frac{2D}{f^2} L(s_m) \frac{\partial \theta}{\partial y} \ , \qquad (3.17)$$

where L(s) is assumed

$$L(s) = \left[\frac{R}{p_m}\left(\frac{p_m}{p_o}\right)^{\kappa}\right] \quad .$$

The equation (3.17) is solved for ψ from the initial temperature field (3.8) with the technique of Ogura and Charney (1962) and v is then determined from (3.16).

It is noted that these initial conditions do not satisfy the boundary conditions on u, v, and θ at the upper and lower boundaries. A period of adjustment will be required to form the surface friction layer and some oscillations may be observed later.

The fields of w and π are obtained through the continuity and hydrostatic equations (2.14) and (2.15).

Finally it is necessary to define explicitly methods used in determining the initial field of specific humidity, given $\Theta_I(y,p,o)$ from equation (3.8).

Saturation vapor pressure e_s, is first determined at each gridpoint through use of an integrated form of the Clausius-Clapeyron equation, an equation expressing saturation vapor pressure as a function of temperature. According to Hess (1959)

$$e_s = .611 \text{ EXP}\left[\frac{L_c}{R_v}\left(\frac{1}{T_o} - \frac{1}{T}\right)\right] , \qquad (3.18)$$

where e_s is expressed in centibars, L_c is the latent heat of condensation, R_v is the gas constant for water vapor, and T_o is a constant of integration.

Knowing saturation vapor pressure, the saturated specific humidity was obtained from the approximated relation from Haltiner and Martin (1957)

$$q_s = \frac{.622e_s}{p} \quad . \tag{3.19}$$

Therefore, by having knowledge of potential temperature at t = 0 from equation (3.8), q_s can be found at each point using equations (3.18) and (3.19). By defining q to be a given fraction of q_s in different experiments, atmospheres of different constant initial relative humidities were tested.

IV. CONVECTIVE ADJUSTMENT, LATENT HEATING AND PRECIPITATION

Inclusion of two additional heating terms in the moist thermodynamic equation (2.3) necessitated some further amendment to W73. Atmospheric heating by dry convective adjustment, Q_A, was included in W73 to eliminate any intense grid scale convection which developed due to the formation of any dry unstable lapse rates. This redistribution of heating was accomplished using averaging techniques to ensure that the dry adiabatic lapse rate was not exceeded $(\frac{\partial \theta}{\partial p} \leq 0)$.

Lapse rates were tested in each vertical column of the model. Upon encountering an unstable layer $(\frac{\partial \theta}{\partial p} > 0)$, a cumulative average was taken and applied to the gridpoints within this layer until neutral stability $(\frac{\partial \theta}{\partial p} = 0)$ was attained. Simultaneously the model was checked for instabilities developing below the convectively adjusted layer and potential temperatures at these levels were also cumulatively averaged and reassigned the new values. The final result of the technique is that the heating is redistributed to simulate physical processes of the atmosphere and mathematically that $\frac{\partial \theta}{\partial p} \leq 0$ throughout each column of the model. A completely analogous scheme was used for saturated parcels in the moist experiment, only using equivalent

potential temperatures, Θ_{sE}, in place of potential temperature, θ.

With the addition of moisture, consideration of large scale condensation and the subsequent release of latent heating became important.

According to Haltiner ( ), changes in moisture and temperature due to large scale condensation were determined as follows. Where relative humidity exceeds 100%, the adjustments in temperature δT and specific humidity δq are determined by the following equations:

$$q + \delta q = q_s(T + \delta T, p) \ , \tag{4.1}$$

and

$$C_p \delta T = - L_c \ \delta q \ . \tag{4.2}$$

These equations require that the final state of the air be exactly saturated and that excess moisture be condensed isobarically, releasing the latent heat to the air.

Equations (4.1) and (4.2) can be expressed in iterative form as

$$\Delta q = q_s(1-r) + \left(\frac{\partial q_s}{\partial T}\right)_p \Delta T \ ; \quad q = r q_s \ , \tag{4.3}$$

and

$$C_p \Delta T = - L \Delta q \ . \tag{4.4}$$

Eliminating ΔT from (4.3) and (4.4) leads to

$$\Delta q = \frac{q_s \ (1-r)}{1 + \frac{L}{C_p} \left(\frac{\partial q_s}{\partial T}\right)} \ . \tag{4.5}$$

At constant pressure the Clausius Clapeyron equation can be expressed as

$$\left(\frac{\partial q_s}{\partial T}\right)_p = \frac{L_c}{R_v}\frac{q_s}{T^2} . \qquad (4.6)$$

Substituting (4.6) into (4.5) we obtain

$$\Delta q = \frac{q_s(1-r)}{1 + \frac{L^2 q_s}{C_p R_v T^2}} . \qquad (4.7)$$

Now Δq may be calculated from (4.7) and the corresponding value of ΔT from (4.4).

The first estimates of the adjusted temperature and specific humidity are, therefore,

$$T' = T + \Delta T \text{ and } q' = q + \Delta q . \qquad (4.8)$$

There values in turn were used to obtain improved approximations. Iterations were contained until the values of T' and q' at each level matched with sufficient accuracy one hundred percent relative humidity. The changes were then applied to the potential temperature and specific humidity fields of the model accounting for the term H_c of equation (2.2) and M_c of equation (2.3)

The model was then investigated for unstable moist convection and its associated heat of condensation. A convective adjustment scheme similar to the dry one was used on the saturated parcels so that moist static stability

was always maintained. A field of equivalent potential temperature was formulated according to Holton (1972) as

$$\Theta_{sE} = \Theta \text{ EXP } \frac{L_c q_s}{C_p T} , \tag{4.9}$$

and the moist convective adjustment was designed to ensure that the moist adiabatic lapse rate was not exceeded ($\partial\Theta_{sE}/\partial p \leq 0$).

The heat release, Q_m, as a result of moist convective adjustment was included through knowledge of the change of equivalent potential temperature during the adjustment.

By taking the natural logarithm of equation (4.9) it is found that

$$\ln \Theta_{sE} = \ln \Theta + \frac{L_c q_s}{C_p T} \tag{4.10}$$

In a model using pressure coordinates, a constant pressure surface may be assumed, so by differentiating both sides of equation (4.10) and recalling the definition of potential temperature gives

$$\frac{d\Theta_{sE}}{\Theta_{sE}} = \frac{dT}{T} + \frac{dq_s L_c}{C_p T} - \frac{L_c q_s dT}{T^2} . \tag{4.11}$$

Solve the Clausius Clapeyron equation (4.6) for dq_s, substitute in equation (4.11), and solve for dT. The

solution is found to be

$$dT = \frac{d\theta_{sE}}{\theta_{sE}\left[\frac{1}{T}\left(1 + \frac{q_s L_c^2}{R_v C_p T^2} - \frac{L q_s}{C_p T}\right)\right]}, \qquad (4.12)$$

where $d\theta_{sE}$ is the change in θ_{sE} needed to adjust $\frac{\partial \theta_{sE}}{\partial p} = 0$.

Since the atmosphere remains saturated throughout this process of moist convective adjustment, the Clausius-Clapeyron equation was again used to obtain the corresponding dq or actually dq_s. Once again the changes were then applied to the potential temperature and specific humidity fields of the model accounting for the term Q_m of equation (2.2) and M_c of equation (2.3).

A cumulative amount of precipitation was then found using the relation

$$p = -\frac{1}{g}\int_{o}^{p_o} \delta q \, dp \qquad (4.13)$$

in agreement with the changes in specific humidity due to condensation and moist convective adjustment. Precipitation was expressed in inches of rainfall in the model.

V. NUMERICAL SOLUTIONS

All numerical results to be shown use the following values for the constant:

Δt = 540 sec p_o = 100 cb p_m = 60 cb H = 80 cb

Δp = 1.78 cb Y = 1800 km Δy = 60 km g = 9.81 m sec^{-2}

f = $10^{-4} sec^{-1}$ D = $10^{-5} sec^{-1}$ θ_o = 300°K

$\Theta_I(p_o)$ = 270, 280, 290, 300°K C_p = 1003 joules $kg^{-1}°K^{-1}$

R_v = 461 joules $kg^{-1}°K^{-1}$ R = 287 joules $kg^{-1}°K^{-1}$

$\kappa = R/C_p$ $L_c = 2.5 \times 10^6$ joules kg^{-1} T_o = 273°K

a =12.56°K RH = 50,70,85%

$\frac{\partial \bar{\Theta}_I}{\partial z}$ = 4°K km^{-1} , $(\frac{\partial \bar{\Theta}_I}{\partial p})_{p_m}$ = -.53448, .6, .8°K cb^{-1}

$A_m = A_\theta = A_q = 3 \times 10^4, 10^5$ $m^2 sec^{-1}$

C_m = 0, .001409, .0001761 $cb^2 sec^{-1}$ (which corresponds to 0, 10, 1.25 $m^2 sec^{-1}$ in height coordinates)

C_θ = 0, .001409, .0001761 $cb^2 sec^{-1}$ (which corresponds to 0, 10, 1.25 $m^2 sec^{-1}$ in height coordinates)

C_q = 0, $cb^2 sec^{-1}$ (which corresponds to 0 $m^2 sec^{-1}$ in height coordinates)

where more than one indicated value means that the constant was varied in different experiments. Whenever possible, the values are the same as those used in W73.

In this section numerical frontogenesis solutions with moisture are examined at t = 4 days and compared to the corresponding dry atmosphere.

As can be seen from Table I, 26 experiments were performed on five cases, cases selected from Williams (1973). Case 1 contains only horizontal turbulent diffusions of momentum, heat, and moisture while cases 2 through 5 contain both horizontal and vertical turbulent diffusions of these parameters. Values chosen for these turbulent diffusion coefficients were computed to correspond with values used in Williams (1973).

In Table I, $\overline{\theta}_I(p_o)$ is the reference potential temperature (°K) as introduced in equation (3.7). The condensation interval indicates the number of time steps between successive applications of condensation and moist convective adjustment to the model. Turbulent diffusion coefficients are then given as previously defined followed by the initial relative humidity (percent) and the initial static stability(°K/cb).

Experiments were first performed with a reference potential temperature ($\overline{\theta}_I(p_o)$) of 300°K to directly compare with the dry solutions of W73. This corresponds to a temperature range of 62-104°F at the surface along a North-South axis. Therefore, experiments were also conducted with $\overline{\theta}_I(p_o)$ = 270,280,290°K to simulate physically realistic situations. Changes to the dry atmosphere with the different references were almost negligible, but due to the exponential function in the Clausius-Clapeyron equation important differences were observed in the moist atmosphere.

Experiments were also conducted using different values for initial relative humidities and initial static stabilities.

A brief tabulation of experimental results is given in Table II, comparing widths of frontal zone, frontal slopes, vertical motions and precipitation.

A reasonable measure of the width of the frontal zone is given by

$$d \equiv \frac{\theta(-Y,s,o) - \theta(Y,s,o)}{\left|\frac{\partial\theta}{\partial y}\right|_{max}} , \qquad (5.1)$$

where $\frac{\partial\theta}{\partial y}$ is approximated by a one-sided difference. This width (km) is indicated at three levels for each experiment in the table.

The North-South location of $\left|\frac{\partial\theta}{\partial y}\right|_{max}$ at three levels is y_f(km) and is used as a position indicator of the frontal zone where $|y_f| \leq 1800$ km.

The pressure level and magnitude of maximum vertical motion is then given followed by the North-South position of maximum precipitation (km), $|y_p| \leq 1800$ km, and the corresponding amounts of cumulative precipitation over the four day period.

It is noted from Table II that widths of frontal zones between corresponding moist and dry experiments are primarily effected at mid to upper levels with only small deviations being noted at the surface. The expected increase of thermal gradient at these mid to upper levels

due to latent heating in the moist cases is seen to be the cause.

Comparisons of frontal slopes of corresponding experiments revealed deviations again at mid levels. The slopes appear more vertical throughout these levels in the moist experiments. Graphical illustrations will later be presented.

Maxima in vertical motion seem to intensify and be found at higher levels along the frontal zone in the corresponding moist cases. This effect can also be directly tied to releases of latent heating in this region.

Cumulative precipitation amounts in Table II are observed to be primarily functions of initial relative humidity and reference potential temperature.

Primary emphasis on analyses of experimental results was on contour plots from the IBM 360/67 computer. These results obtained for all 26 experiments are analyses at $t = 4$ days of the fields of u, q, θ' and w where $\theta' = \theta - \overline{\theta}_I$ and $\overline{\theta}_I$ is the horizontally averaged initial potential temperature. The entire vertical plane is shown from 100 to 20 cb in these plots. However, the outer portion of the domain between $|y| = 1200$ km and $|y| = 1800$ km is not shown. Also note that isolines of specific humidity in the figures to follow have different intervals dependent upon reference potential temperatures in order to allow for proper definition of the field.

Due to the large number of contour plots obtained, experiments 1,2,4,5,6,11,12,13,17,18 were chosen as representative samples for detailed discussion. Experiments 1,2,4,5,6 and 11 contain only horizontal turbulent diffusions of momentum, heat, and moisture while experiments 12,13,17 and 18 contain both horizontal and vertical turbulent diffusions of these parameters.

Figure 1 comparing experiments 1 and 2 shows the frontal scale at 99.1 cb reaching steady-state at approximately t = 2 days. Little deviation is seen between the wet and dry experiment. Figure 2 compares the frontal slopes of the same two experiments. As mentioned before slopes are seen to be largely the same with the only significant deviation being at midlevels where the moist slopes approaches the vertical and then recurves in agreement with the dry solution.

Again this deviation in the wet experiment is probably due to the release of latent heating at these levels. Similar results were achieved for other cases with more extreme deviations being observed at higher reference potential temperatures.

Contour plots for experiments 1 and 2 are shown as figures 5 - 12. Figures 5 and 6 show distributions of the rotational wind, u for a corresponding dry and moist experiment respectively. It is noted that low level features are quite similar in the easterly flow. However, horizontal

and vertical wind shear is more intense at low mid to mid levels in the warm air in the moist experiment. It is noteworthy that this property is dominant throughout the moist solution.

Figures 7 and 8 contrast values of θ' throughout the domain. Noted is the more intense gradient of potential temperature through the mid levels and the pocket of warm air at mid levels most likely due to release of latent heating in the moist experiment.

Fields of specific humidity are contrasted for experiments 1 and 2 in figures 9 and 10. In the dry experiment moisture is merely advected and horizontally diffused throughout the domain showing an interesting though physically unrealistic situation. The processes of condensation and moist convective adjustment are only applied in the moist experiments. By comparing the isolines of specific humidity, it is seen that the processes of condensation and convective adjustment are indeed reducing the moisture content of the air and that the gradient of specific humidity is stronger along the frontal zone in the dry experiment where no condensation is taking place.

Vertical motions are investigated for the experiments in figures 11 and 12. Upward vertical motions are stronger and occur at higher levels closer to the frontal zone in the warm air mass for the moist experiment. Downward vertical motion in the cold air mass was also slightly intensified with its maximum also at a higher level.

Figures 13 - 28 compare the dry and moist fields of u, q, θ' and w at reference potential temperatures of 290, 300 and 270°K. Figures 13 - 16 show moist fields ($\bar{\theta}_I(p_o)$ = 290°K). The horizontal and vertical shear of u in figure 13 is seen to be stronger and to be extending to higher levels than in the previous moist experiment. Stronger thermal gradients are seen to extend higher in the atmosphere in figure 14. Latent heat release occurs at higher levels and to greater extent as is seen in the upper level isentropic pattern to the warm air side of the frontal zone.

As is predicted by the Clausius-Clapeyron equation (3.18), the moisture values (figure 15) are significantly greater than in the previous experiments. Again note the decreased gradient of moisture along the frontal zone in the moist experiment.

Vertical motions, shown in figure 16, are also somewhat intensified, occur at higher levels and have slightly more intense gradients along the discontinuity in the warm air. The downward vertical motions in the cold air are also somewhat increased.

Figures 17 - 24 contrast dry and moist experiments with a reference potential temperature of 300°K. Little difference is seen between the dry experiment and the earlier dry fields based on 280°K except for a northward displacement of the fields at the colder reference potential temperature. Due to the exponential nature of the

moisture parameter, moist fields showed significant changes in the following experiments.

The rotational wind u, as is shown in figures 17 and 18, has much stronger horizontal and vertical shear in the warm air at low mid to upper levels than in previous moist experiments and even has an area of easterly winds at upper levels in the warm air. The air is much warmer in the upper levels due to latent heat release, as indicated by figures 19 and 20. Thermal gradients along the frontal zone in the warm air are also stronger in the mid and upper levels.

Gradients in the moisture field are greatly intensified and specific humidities are in excess of 28 g/kg at low levels to the South. Recall that the "dry" q field (figure 21) is distributed due to advective and horizontal diffusive processes only. Perturbations in the moist experiment (figure 22) are probably due to the larger quantities of latent heat release observed in this experiment.

Vertical motions (figures 23 and 24) exceed 4×10^{-3} mb/sec in the warm moist air. These features occur at upper levels and a cell containing downward motion is observed at these upper levels to the South and seems to be somewhat due to the impermeable upper boundary.

Fields with a reference potential temperature of 270°K are finally examined in figures 25 - 28. Due to minimal moisture content at these lower temperatures the fields are quite comparable to dry experiments previously shown.

Shear in the u field (figure 25) and thermal characteristics (figure 26) are also quite similar to dry experiments. Specific humidity (figure 27) reaches a maximum of 5 g/kg allowing for only a small possible latent heat release. Finally, vertical motions (figure 28) occur mainly at the lower levels and are more closely tied to dry experiments.

Further experiments with case 1 are included in Table I. Due to the repetitive nature of the contour plots obtained, they are not included as figures, but some further discussion is appropriate at this time.

Experiments 3 and 8 were run with varying initial relative humidities. Higher initial humidities do lead to more latent heat release with its increased thermal gradients, wind shear, and vertical motion in the warm air but did not seem to warrant further experimentation.

Experiments 9 and 10 were run with varying static stabilities but due to extensive similarities in the solutions, further experiments were not required.

The condensation interval was generally five time steps. The iterative procedure of returning relative humidities to 100% worked equally well at every ten time steps, never exceeding two iterations. However, five time steps were finally chosen to compromise computer time and physical reality. Only minor changes were observed in the contour plots of u, q, θ' and w.

Experiments that follow contain both horizontal and vertical turbulent diffusions of momentum, heat, and moisture. As in the horizontal case previously discussed, values of the diffusion coefficients were computed to correspond with those used in Williams (1973).

Figure 3 compares the frontal slopes for the corresponding dry and moist experiments 12 and 13. Once again, slopes are almost identical with the exception of at mid-levels, where in the moist experiment maximum potential temperature gradient again shifts toward the warm air and then recurves to agree with the dry experiment.

Figure 4 for the same experiments shows frontal scale at 99.1 cb versus time with steady-state being obtained at approximately t = 2 days. Oscillations arise from the development of the surface boundary layer, which is not present in the initial conditions as was described in Williams (1973). Very little difference is observed between the moist and dry solutions at low levels which reinforces the idea that the model remains essentially unchanged at these levels with addition of moisture.

Contour plots are then shown as figures 29 - 36 for experiments 12 and 13. Compared to the corresponding dry case, horizontal and vertical wind shear is again increased especially at low mid to upper mid levels in the warm air (figures 29 and 30). The thermal pattern (figures 31 and 32) shows increased gradient at the low mid to upper levels

in the warm air and the area of maximum latent heat release is seen in the isentropic pattern. Vertical influences for the moist experiment seem somewhat more pronounced for a reference potential temperature of 280°K as compared with similar experiments containing only horizontal diffusion.

Figures 33 and 34 compare the fields of specific humidity. The changes continue to be a reduction in gradient along the frontal zone in the prime area of latent heat release in the moist experiment. Little change is observed throughout the rest of the domain.

Vertical motion fields (figures 35 and 36) for these same experiments show low level maxima of 1.5×10^{-3} mb/sec in the warm air but an additional more intense maximum of vertical motion is found at mid and mid upper levels along the frontal zone in the moist experiment.

Case 3 includes a vertical thermal turbulent diffusion coefficient eight times as large as in case 2 previously discussed. From Williams (1973) a decrease in frontal tilt is expected along with an increase of frontal scale due to the change in diffusion coefficients. This can be observed by comparing appropriate figures of the dry atmosphere. Other changes to the fields will most likely be due to inclusion of moisture. At any rate our comparisons will remain as before, a comparison between the corresponding dry and moist experiments.

Figures 37 and 38, comparing experiments 17 and 18, show again the increase of horizontal and vertical wind

shear at low mid to upper mid levels to slightly greater extent than in the previous moist experiment, experiment 30.

The isentropic analyses (figures 39 and 40) show the tightening of potential temperature gradient at low mid to upper levels once again. However, it is now observed that the increased thermal diffusion has smoothed somewhat the perturbation in the isentropes in the area of maximum latent heat release. This added vertical thermal diffusion seems to aid in distributing the isolated heating induced "pocket" that had been noted previously.

Figures 41 and 42 compare specific humidity fields of the same experiments showing the weakening of gradients at low mid to upper levels due to condensation.

The fields of vertical motion, figures 43 and 44, are similar in results to the previously discussed experiment containing horizontal and vertical turbulent diffusions except for some smoothing of features due to the added vertical thermal diffusion of the present experiment. Once again the maxima noted in the dry experiment 18 is maintained with an added maximum in vertical motion in the mid level warm air along the frontal zone in the moist experiment.

After an analysis of the before mentioned experiments, it becomes obvious that an observational pattern has developed and that further discussion using the line of attack would be largely repetitive.

Careful analysis of the contour plots of the remaining of the 26 experiments contained essentially the same features as those discussed herein.

VI. CONCLUSIONS AND RECOMMENDATIONS

The numerical model of Williams (1973) is modified in this study to include moisture. The numerical solutions become quasi-steady within 1-2 days as in W73. Intensification of the baroclinic zone at mid to upper levels seems to be the significant addition to the model due to the inclusion of moisture. This intensification of the baroclinic zone at the mid to upper levels is consistently manifested by the increases of thermal gradient, wind shear, and vertical motions in the warm air along the frontal zone which are due to latent heat release. Secondly, it should be noted that the model is essentially unchanged at low levels with the inclusion of moisture. Thirdly, the model with moisture shows dependence upon the reference potential temperature, $\theta_I(p_o)$ chosen due to the exponential relationship between moisture and temperature as is indicated by the Clausius-Clapeyron equation (3.18). It is recalled that the dry model is relatively insensitive to choice of this reference temperature. The moist model illustrates this exponential thermal dependence in the various experiments at the reference potential temperatures of 270, 280, 290, and 300°K.

In future studies using Williams model, attention should be directed towards transformation to ln p

coordinates for a better depiction of upper level gradients. Upper level boundaries might also be changed and raised to include a stratosphere and finally a more sophisticated convective scheme might be applied to the model such as that of Arakawa and Schubert (1973).

TABLE I. Listing of Experiments

EXP NO.	CASE NO.	$\overline{\theta}_I(p_o)$ °K	MOIST OR DRY	CON INTER	A_m m^2/sec	A_θ m^2/sec	A_q m^2/sec	C_m cb^2/sec	C_θ cb^2/sec	C_q cb^2/sec	RH %	$\partial\overline{\theta}_I/\partial p$ °K/cb
1	1	280	D	-	100,000	100,000	100,000	0	0	0	70	-.53
2	1	280	M	5	100,000	100,000	100,000	0	0	0	70	-.53
3	1	280	M	5	100,000	100,000	100,000	0	0	0	85	-.53
4	1	290	M	5	100,000	100,000	100,000	0	0	0	70	-.53
5	1	300	D	-	100,000	100,000	100,000	0	0	0	70	-.53
6	1	300	M	5	100,000	100,000	100,000	0	0	0	70	-.53
7	1	300	M	10	100,000	100,000	100,000	0	0	0	70	-.53
8	1	300	M	5	100,000	100,000	100,000	0	0	0	50	-.53
9	1	300	M	5	100,000	100,000	100,000	0	0	0	70	-.60
10	1	300	M	5	100,000	100,000	100,000	0	0	0	70	-.80
11	1	270	M	5	100,000	100,000	100,000	0	0	0	70	-.53
12	2	280	D	-	30,000	30,000	30,000	.001409	.0001761	0	70	-.53
13	2	280	M	5	30,000	30,000	30,000	.001409	.0001761	0	70	-.53
14	2	290	M	5	30,000	30,000	30,000	.001409	.0001761	0	70	-.53
15	2	300	D	-	30,000	30,000	30,000	.001409	.0001761	0	70	-.53
16	2	300	M	5	30,000	30,000	30,000	.001409	.0001761	0	70	-.53
17	3	280	D	-	30,000	30,000	30,000	.001409	.001409	0	70	-.53
18	3	280	M	5	30,000	30,000	30,000	.001409	.001409	0	70	-.53
19	3	300	D	-	30,000	30,000	30,000	.001409	.001409	0	70	-.53
20	3	300	M	5	30,000	30,000	30,000	.001409	.001409	0	70	-.53
21	4	300	D	-	100,000	100,000	100,000	.001409	.0001761	0	70	-.53
22	4	300	M	5	100,000	100,000	100,000	.001409	.0001761	0	70	-.53
23	4	280	D	-	100,000	100,000	100,000	.001409	.0001761	0	70	-.53
24	4	280	M	5	100,000	100,000	100,000	.001409	.0001761	0	70	-.53
25	5	280	D	-	100,000	100,000	100,000	.001409	.001409	0	70	-.53
26	5	280	M	5	100,000	100,000	100,000	.001409	.001409	0	70	-.53

TABLE II. Synopsis of Experimental Results

EXP NO.	CASE NO.	d_{100cb} km	d_{60cb} km	d_{20cb} km	y_{f100cb} km	y_{f60cb} km	y_{f20cb} km	w_{max} ($\times 10^{-3}$ mb/sec)	Level w_{max} cb	p_{max} in	y_{pmax} km
1	1	185	1048	218	-510	90	690	1.21	80.4	-	-
2	1	177	783	206	-510	-90	690	3.22	68.0	.23	-330
3	1	172	729	215	-510	-90	750	3.83	74.3	.35	-390
4	1	185	713	198	-510	-150	750	3.74	55.7	.44	-270
5	1	193	1093	216	-510	90	630	1.13	82.2	-	-
6	1	194	613	127	-510	-90	870	4.26	48.4	.68	-210
7	1	193	474	134	-510	-90	870	3.36	60.9	.54	-210
8	1	194	610	201	-510	-90	750	2.64	50.2	.22	-150
9	1	190	546	130	-450	-90	870	4.12	44.9	.64	-210
10	1	187	530	137	-450	-90	870	4.48	53.8	.60	-210
11	1	173	869	201	-510	90	690	2.28	74.3	.10	-330
12	2	237	1181	274	-930	150	810	1.66	91.1	-	-
13	2	221	726	266	-870	-90	870	3.76	68.0	.23	-270
14	2	217	560	222	-870	-90	930	4.68	37.3	.46	-210
15	2	252	1223	304	-930	150	810	1.60	89.3	-	-
16	2	219	360	141	-870	-90	1110	6.67	39.1	.75	-210
17	3	538	1326	414	-750	270	630	2.72	87.7	-	-
18	3	443	942	349	-690	-150	750	3.89	60.9	.27	-330
19	3	555	1350	394	-690	270	630	2.64	87.7	-	-
20	3	462	381	210	-630	-90	930	5.84	36.0	.62	-150
21	4	366	1291	416	-870	210	750	1.36	89.3	-	-
22	4	335	623	209	-870	-90	1050	5.48	50.2	.74	-210
23	4	362	1244	388	-870	210	810	1.42	89.3	-	-
24	4	329	851	390	-870	-90	810	3.28	66.2	.22	-330
25	5	614	1376	497	-690	210	630	2.26	82.7	-	-
26	5	541	1011	436	-630	-150	690	3.42	66.2	.25	-330

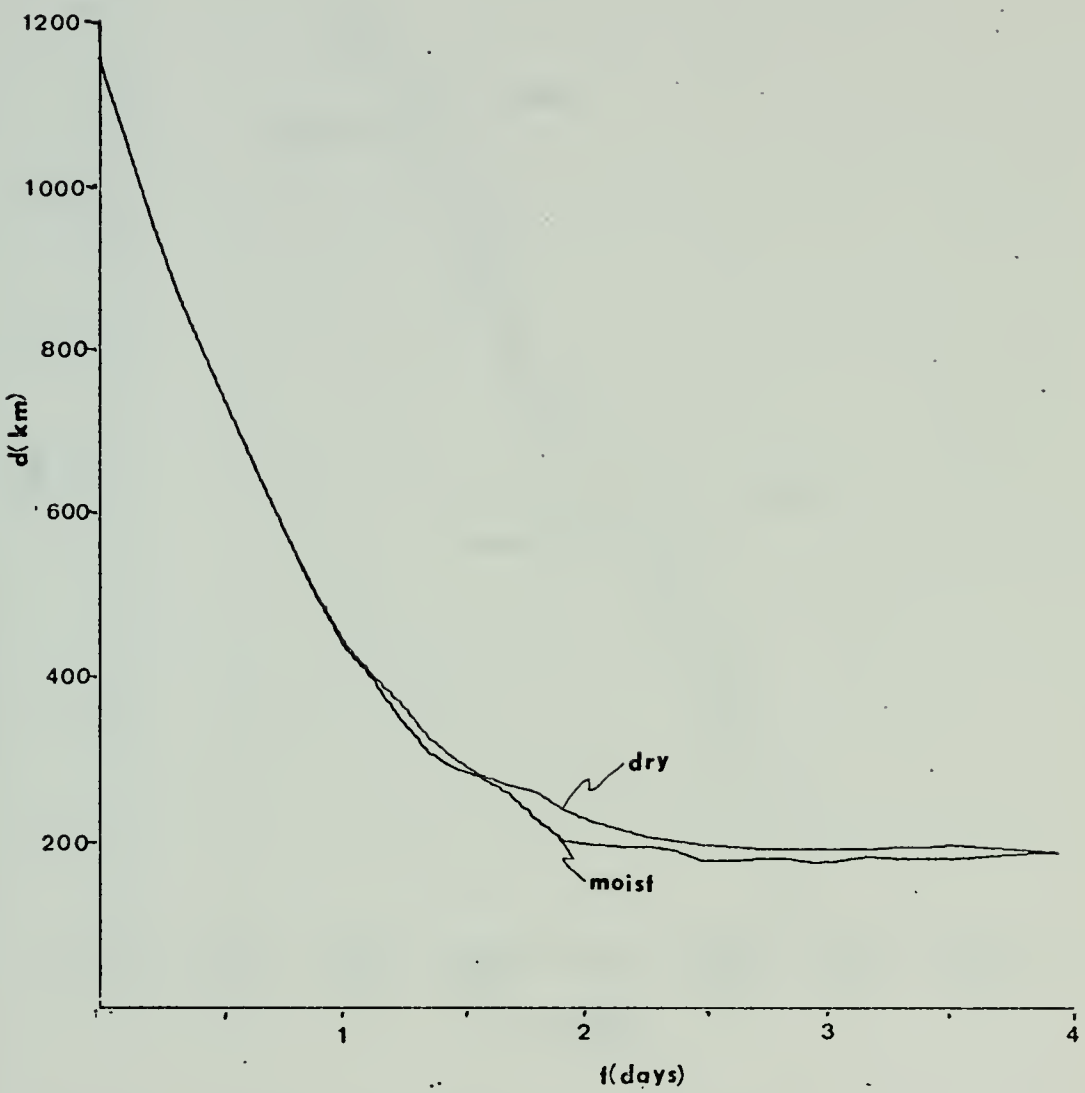

Figure 1. Frontal scale. Experiments 1 and 2.

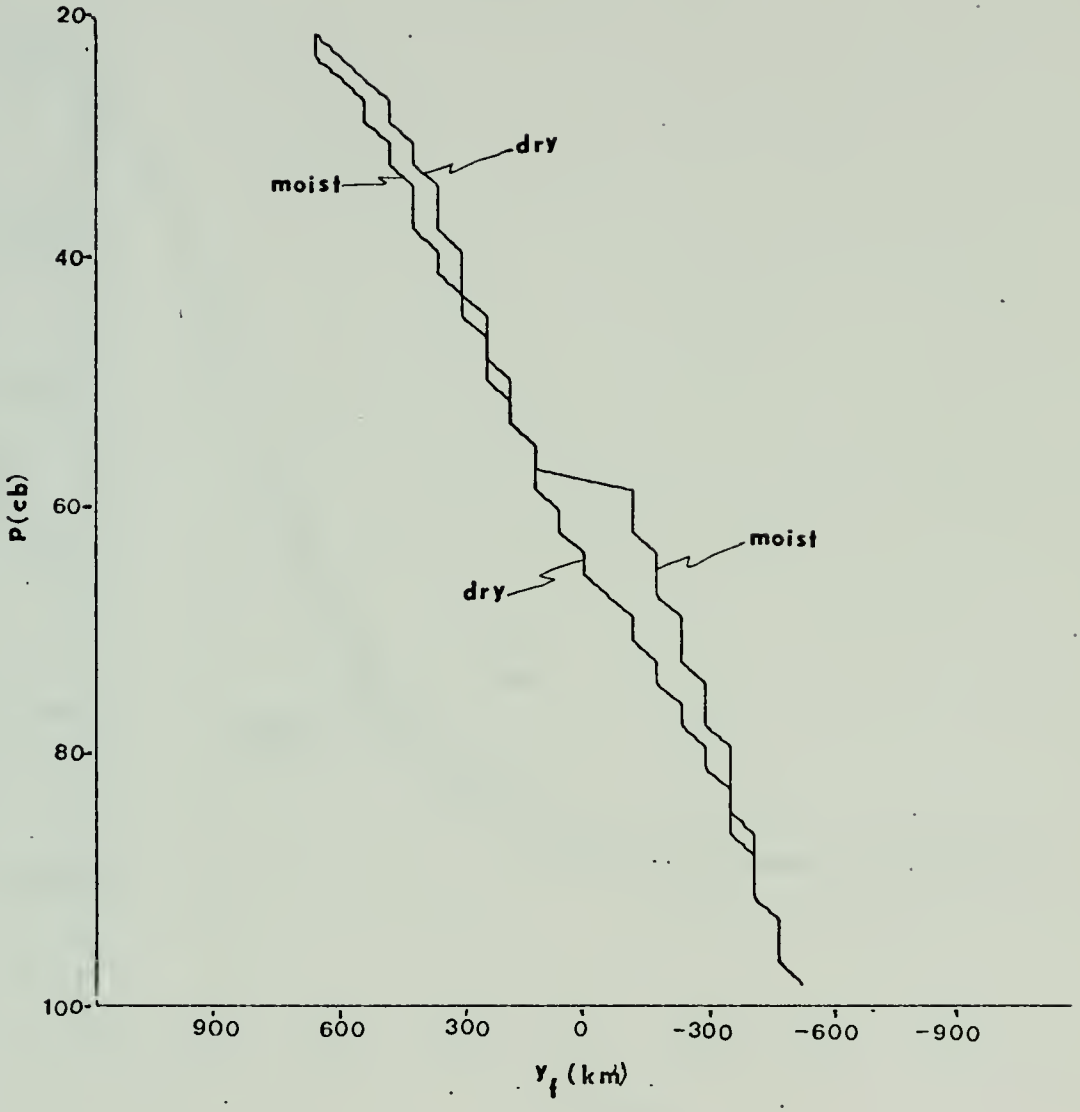

Figure 2. Frontal slope. Experiments 1 and 2.

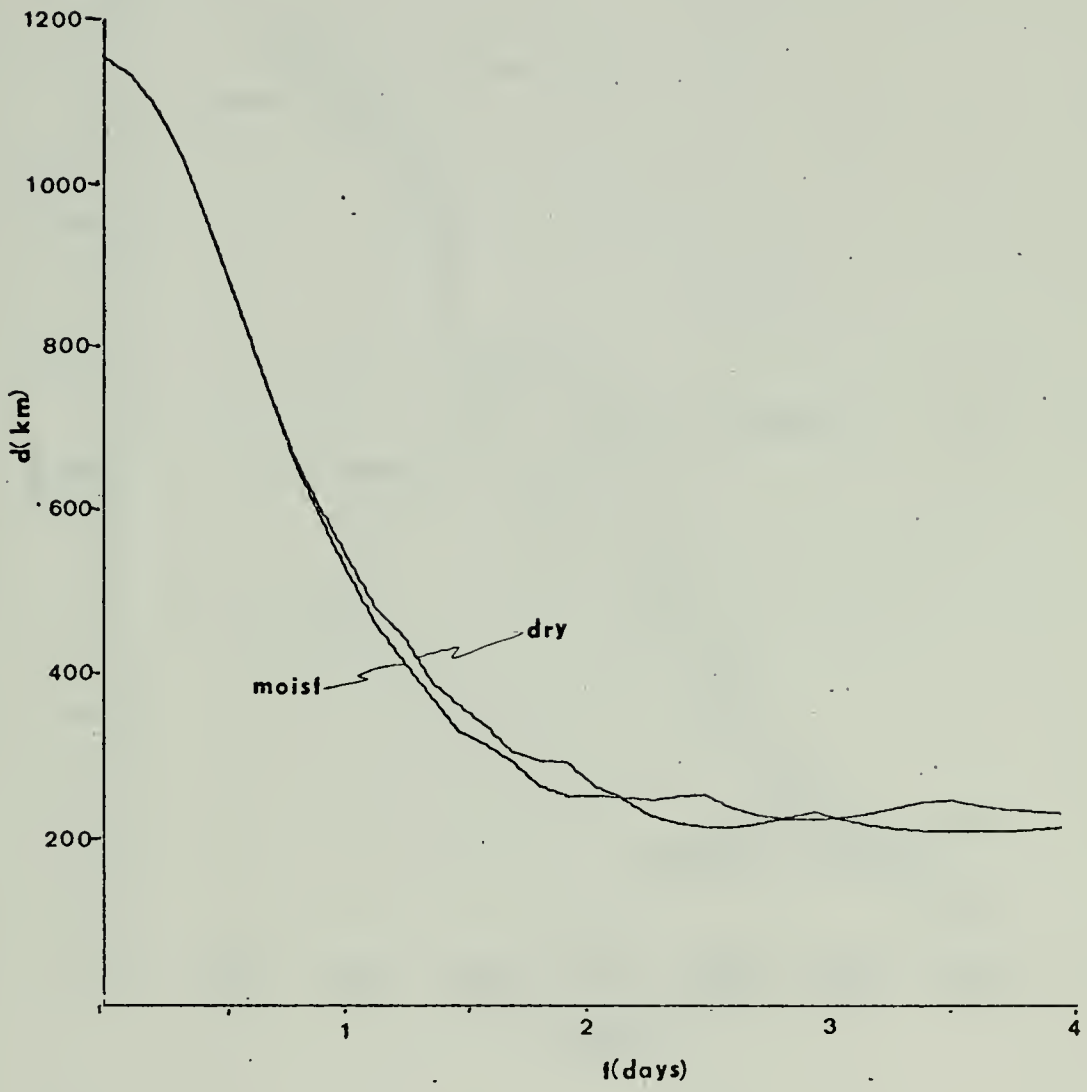

Figure 3. Frontal scale. Experiments 12 and 13.

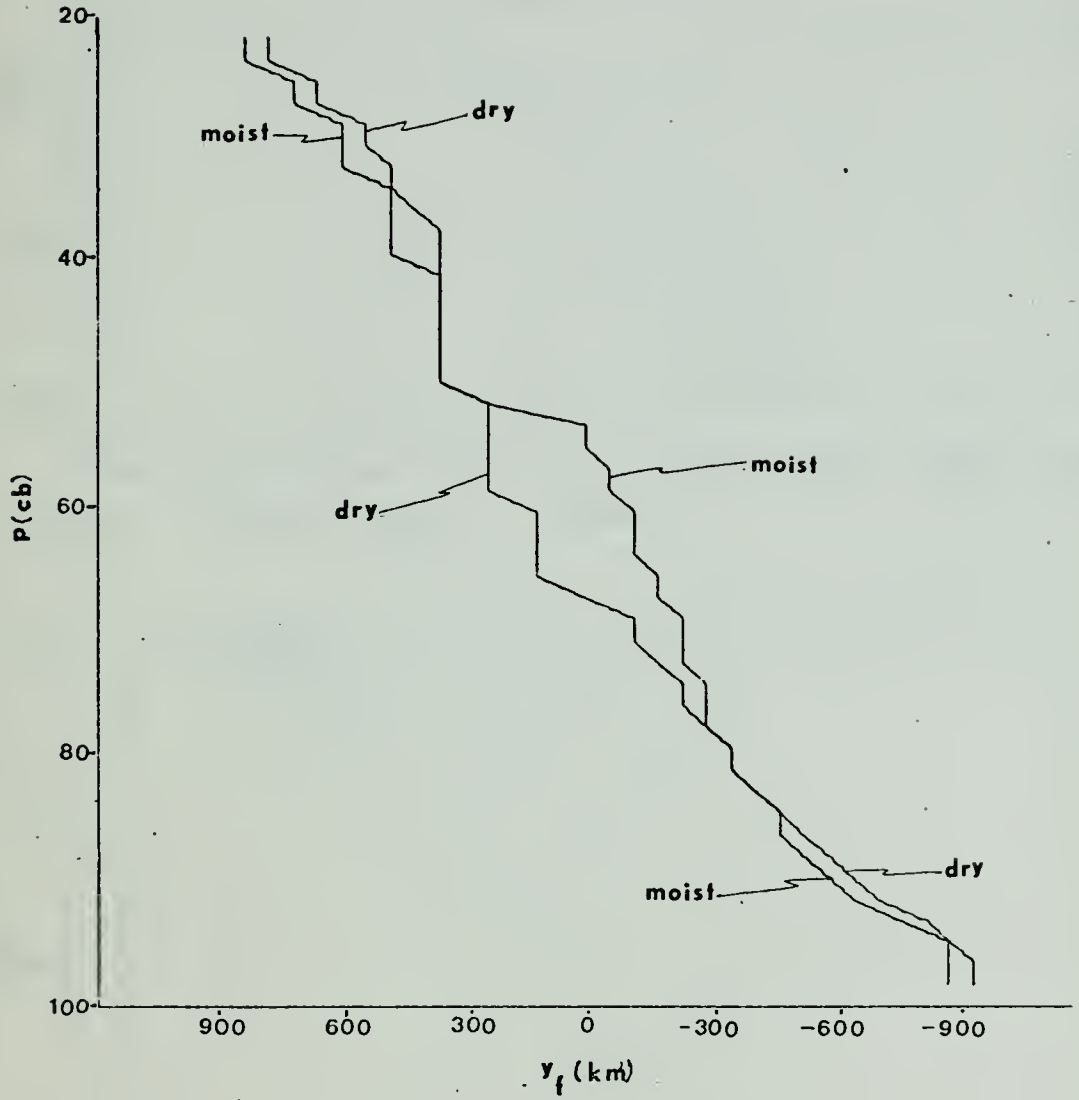

Figure 4. Frontal slope. Experiments 12 and 13.

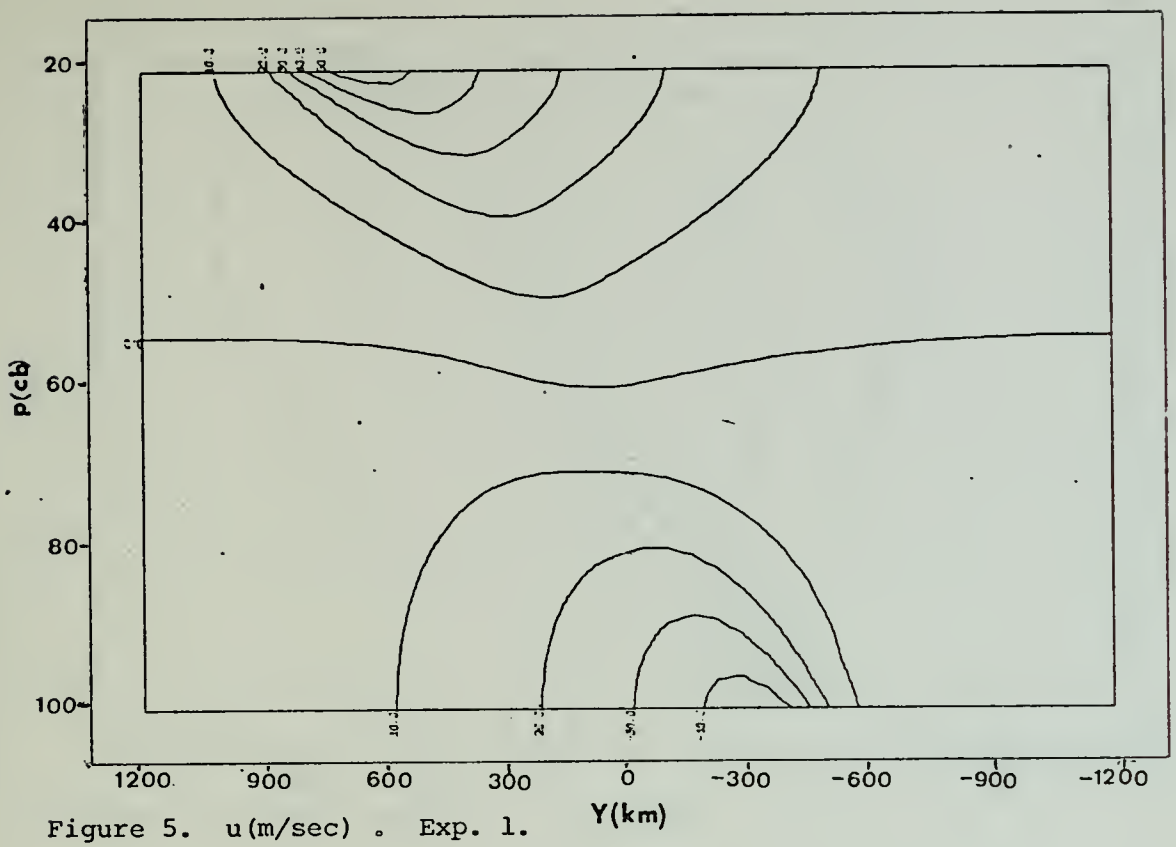

Figure 5. u(m/sec) . Exp. 1.

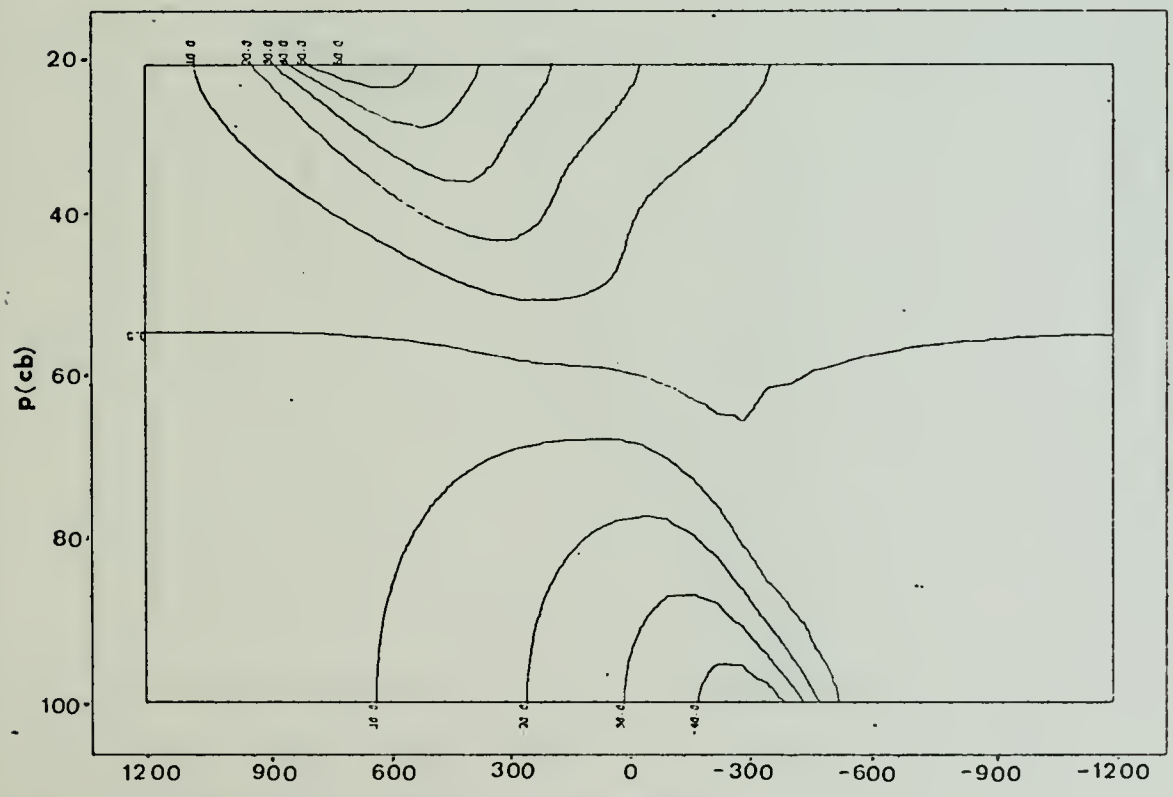

Figure 6. u(m/sec) . Exp. 2.

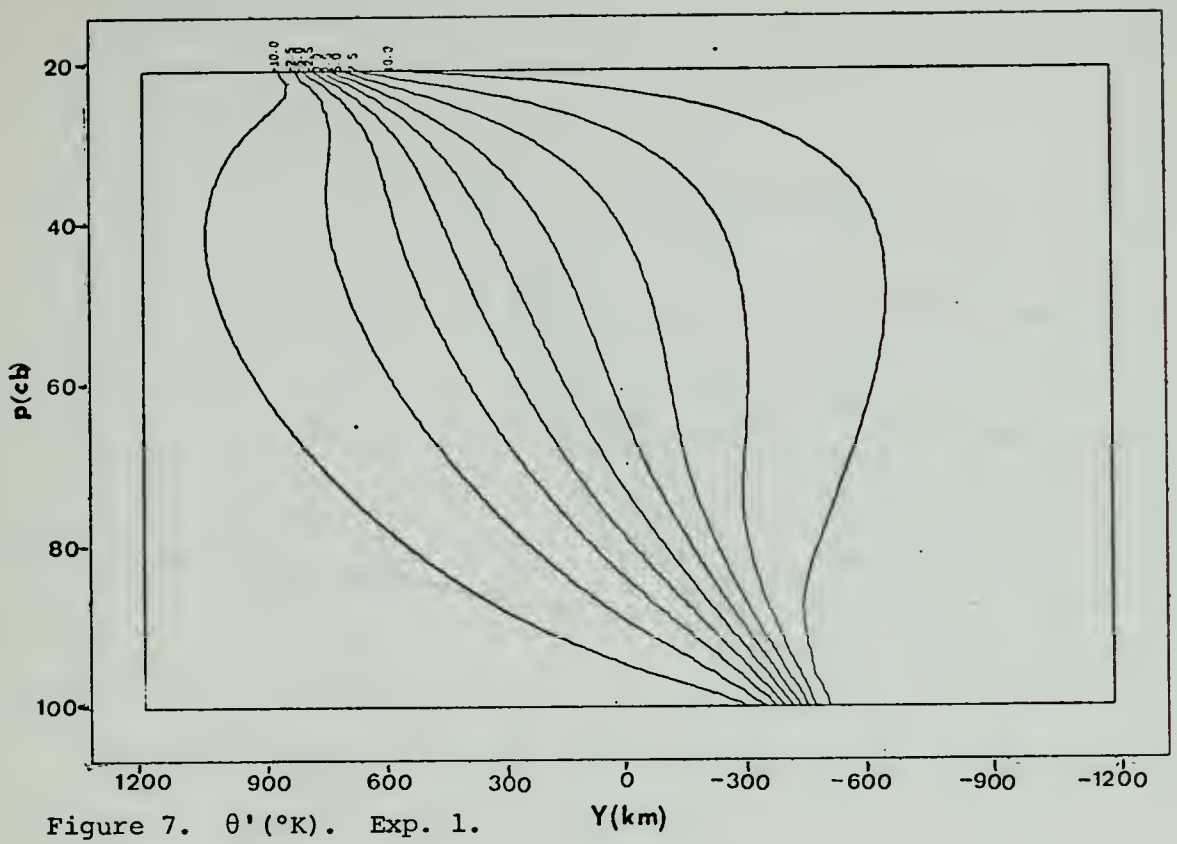

Figure 7. θ'(°K). Exp. 1.

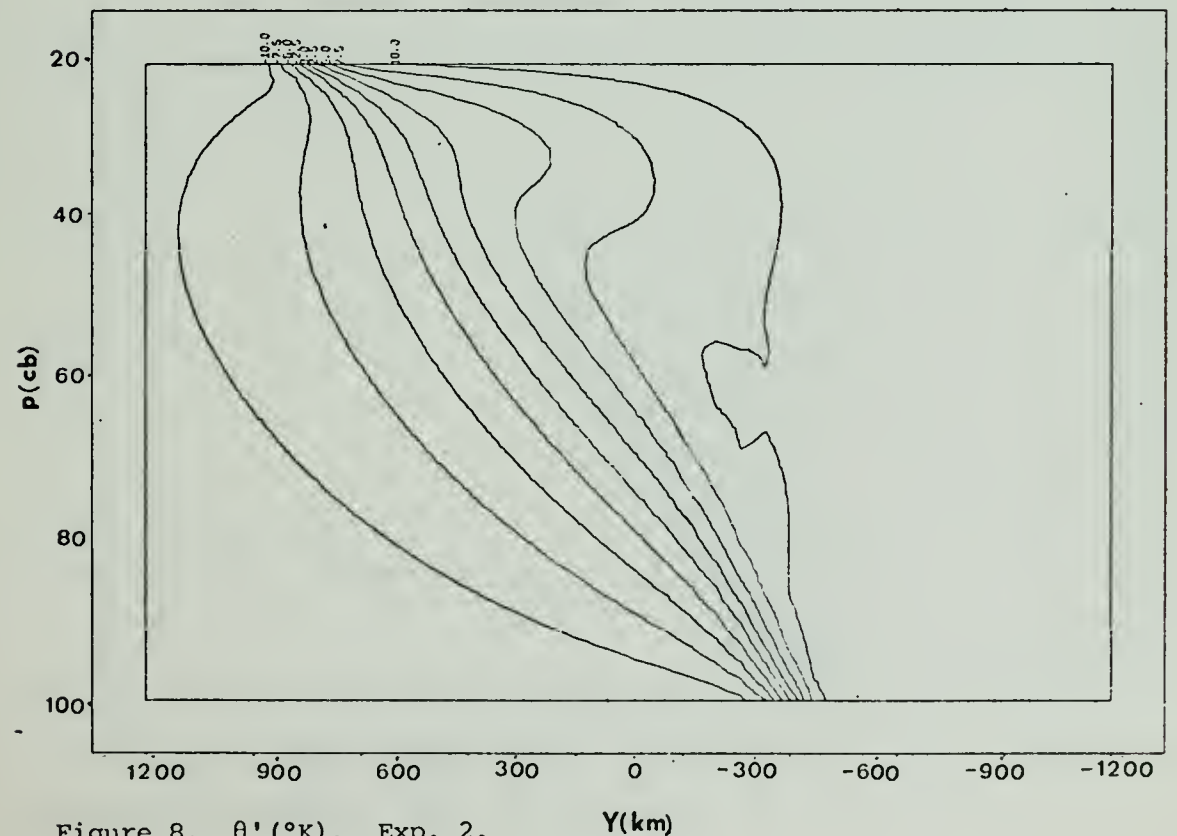

Figure 8. θ'(°K). Exp. 2.

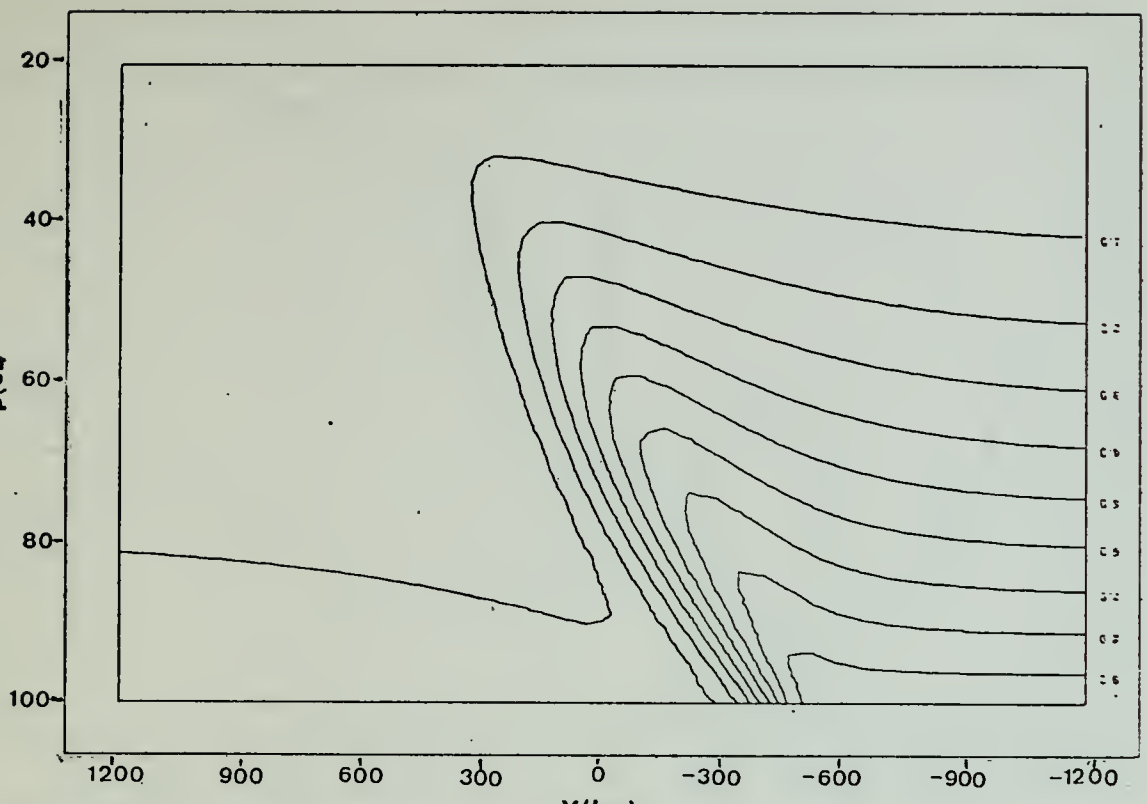

Figure 9. q(g/kg). Exp. 1.

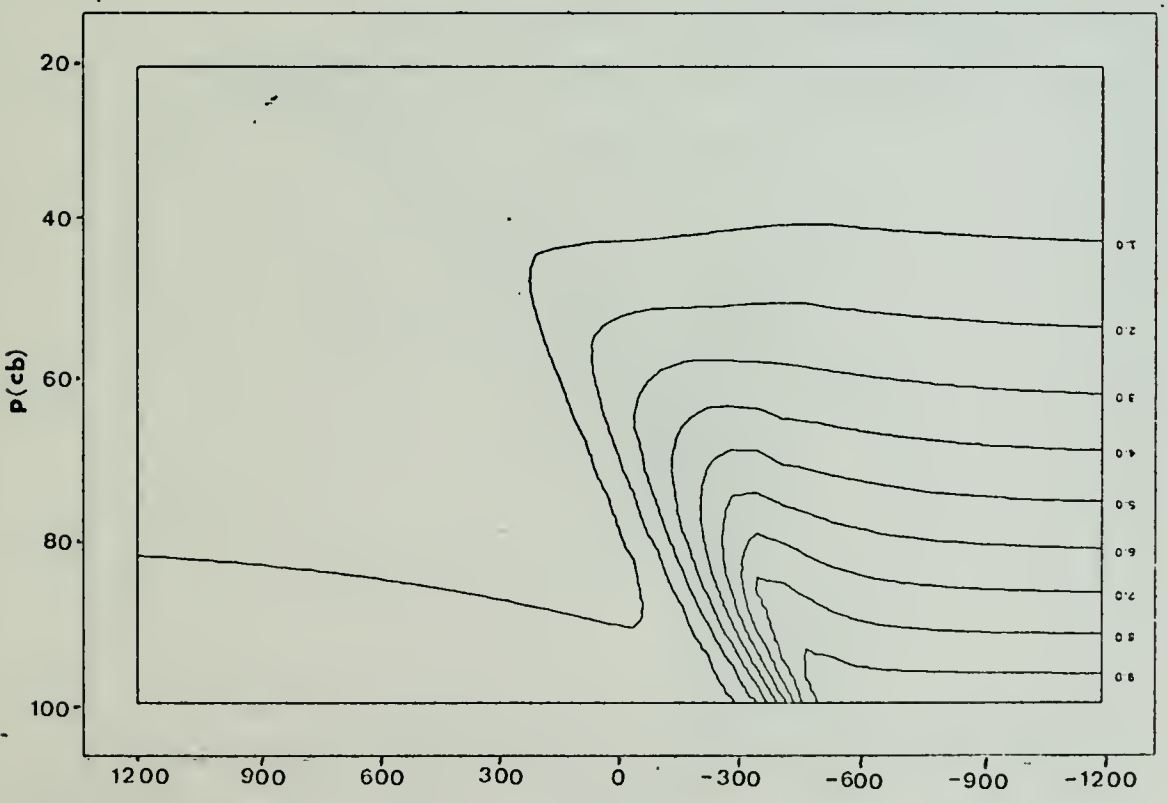

Figure 10. q(g/kg). Exp. 2.

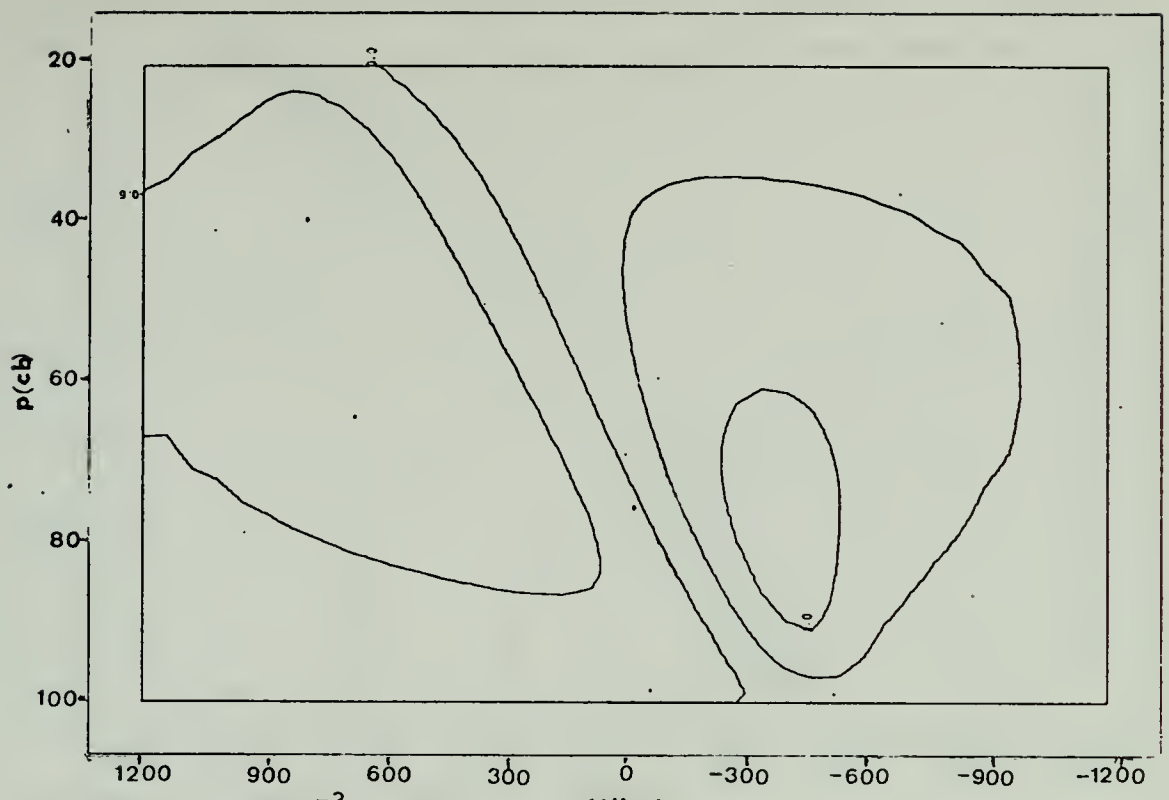

Figure 11. w(x10^{-3}mb/sec). Exp.1.

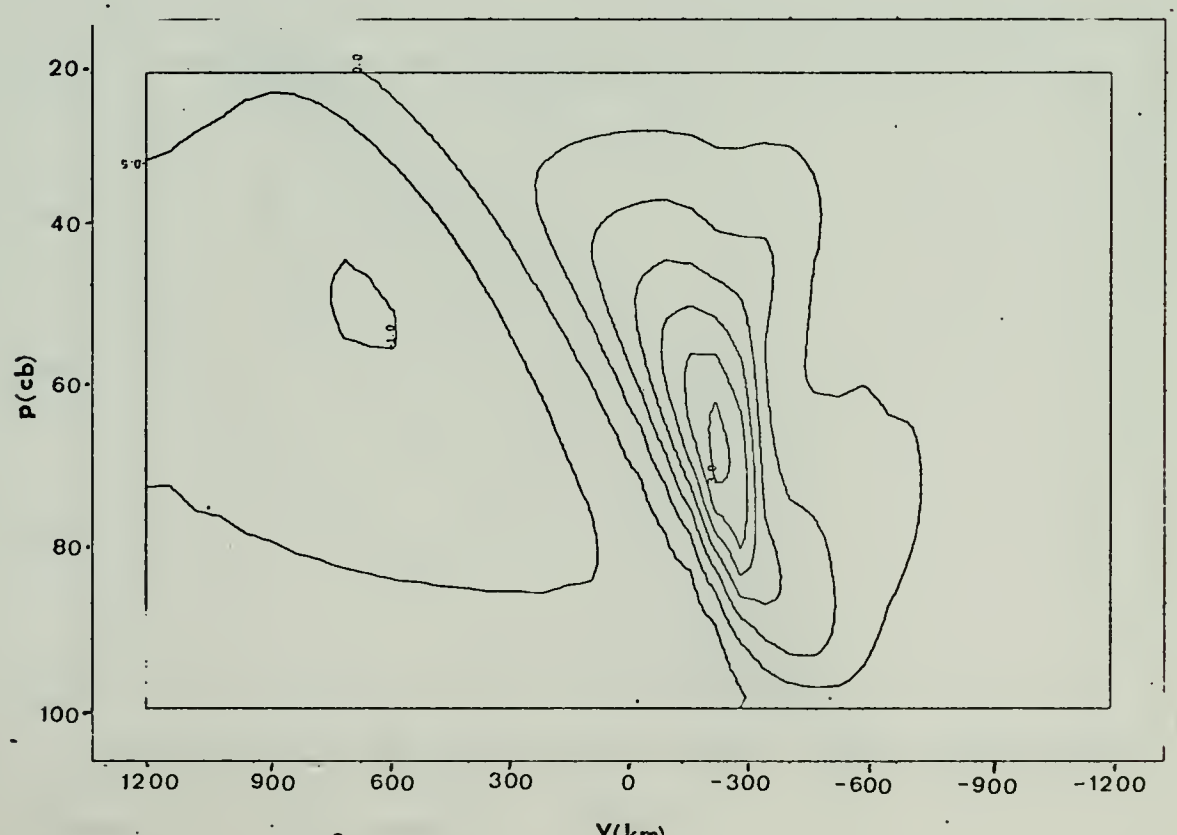

Figure 12. w(x10^{-3}mb/sec). Exp. 2.

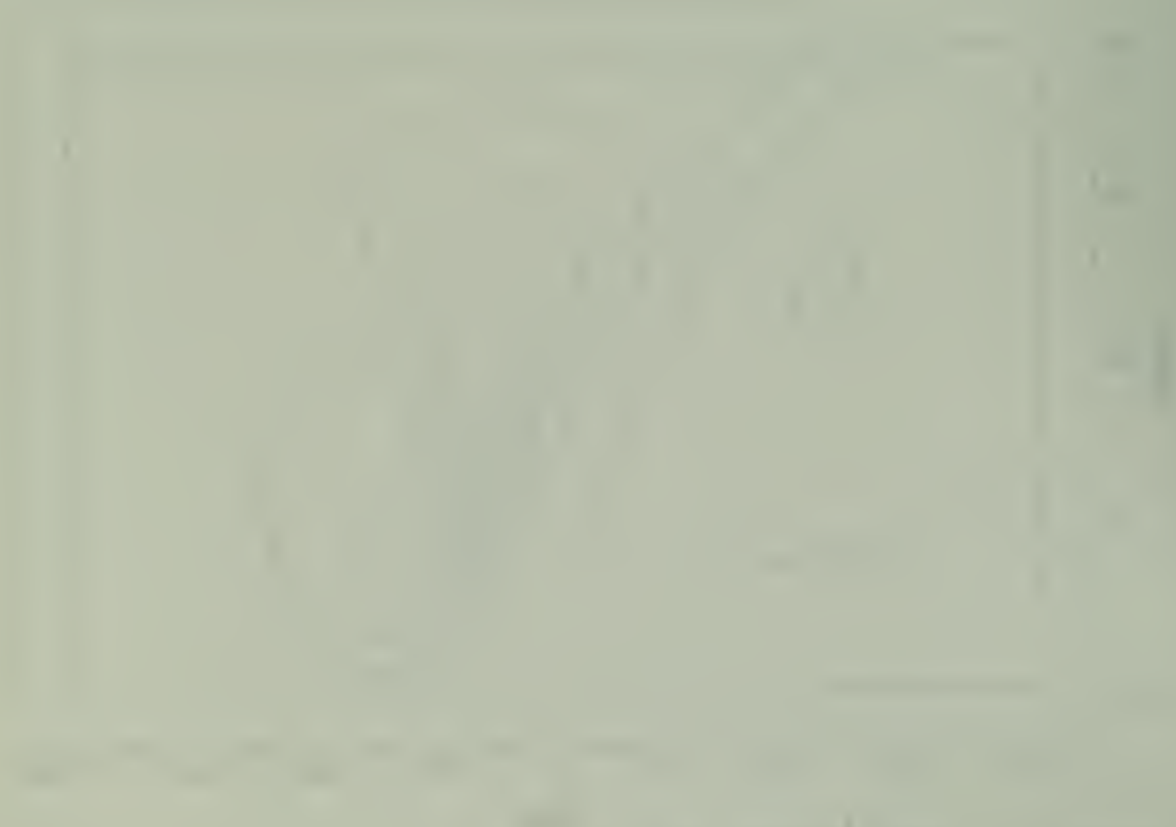

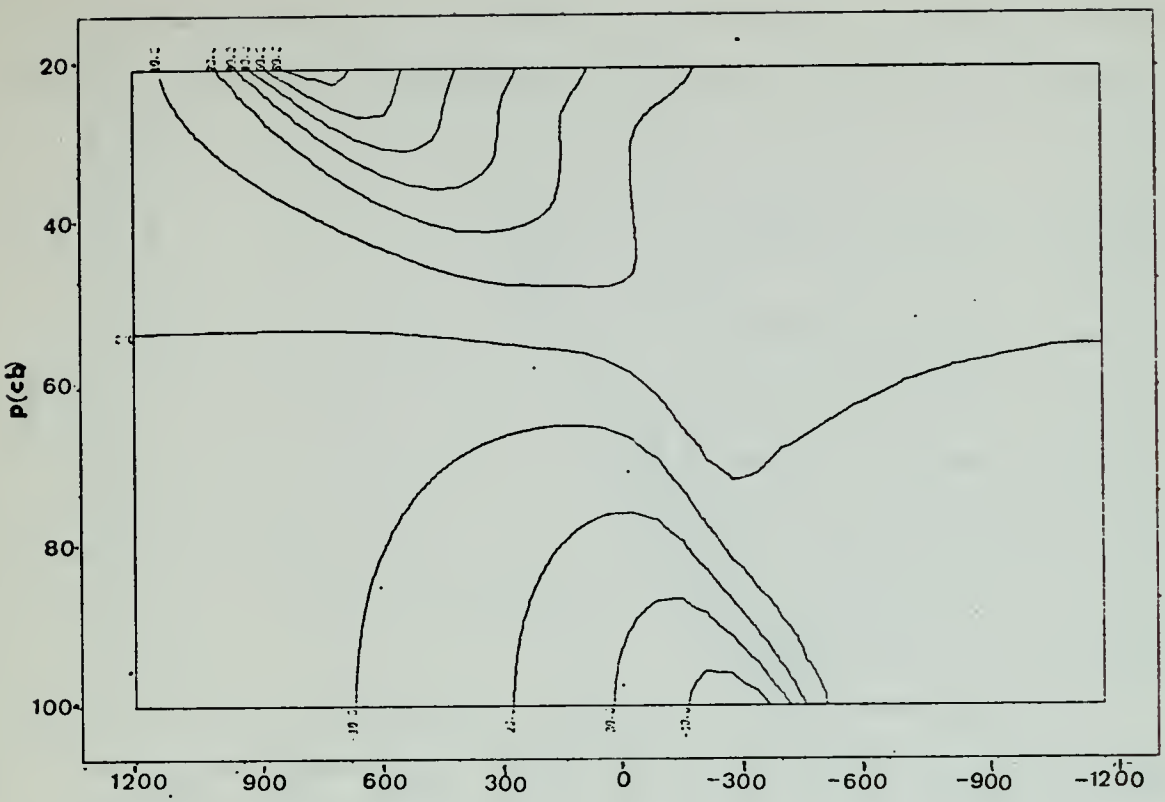

Figure 13. u(m/sec). Exp. 4.

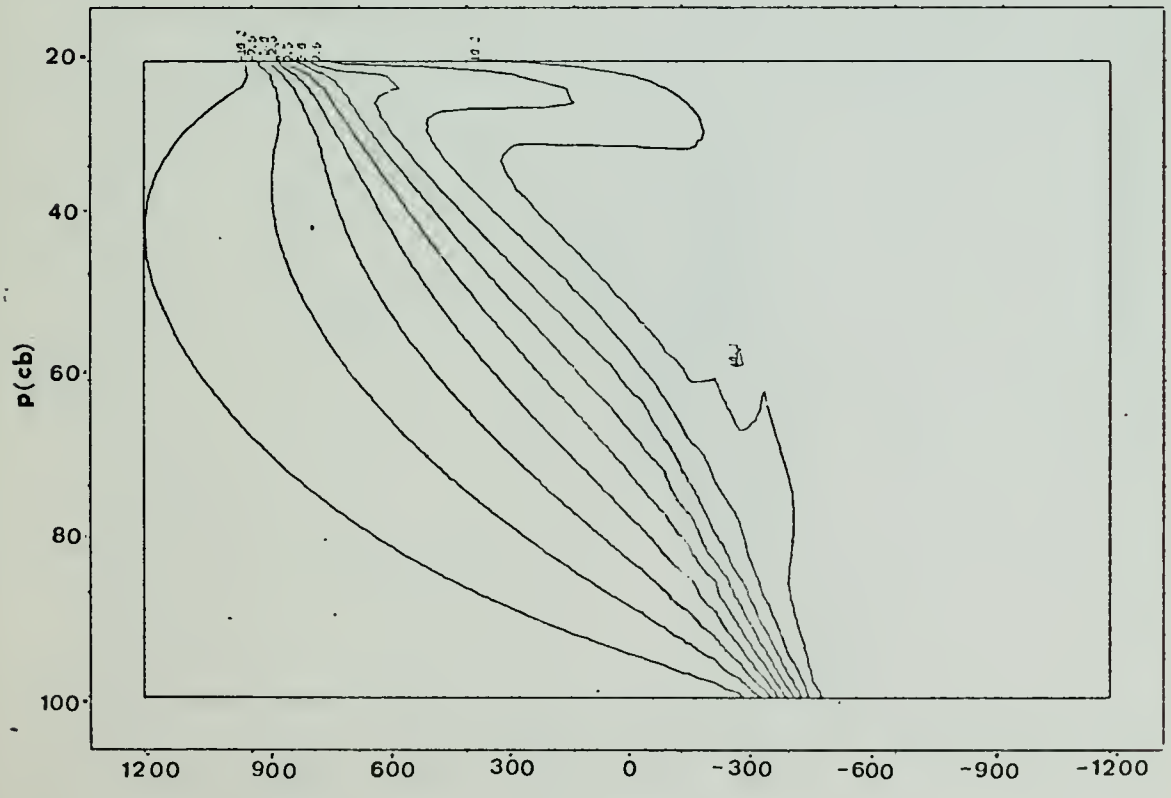

Figure 14. θ'(°K). Exp. 4.

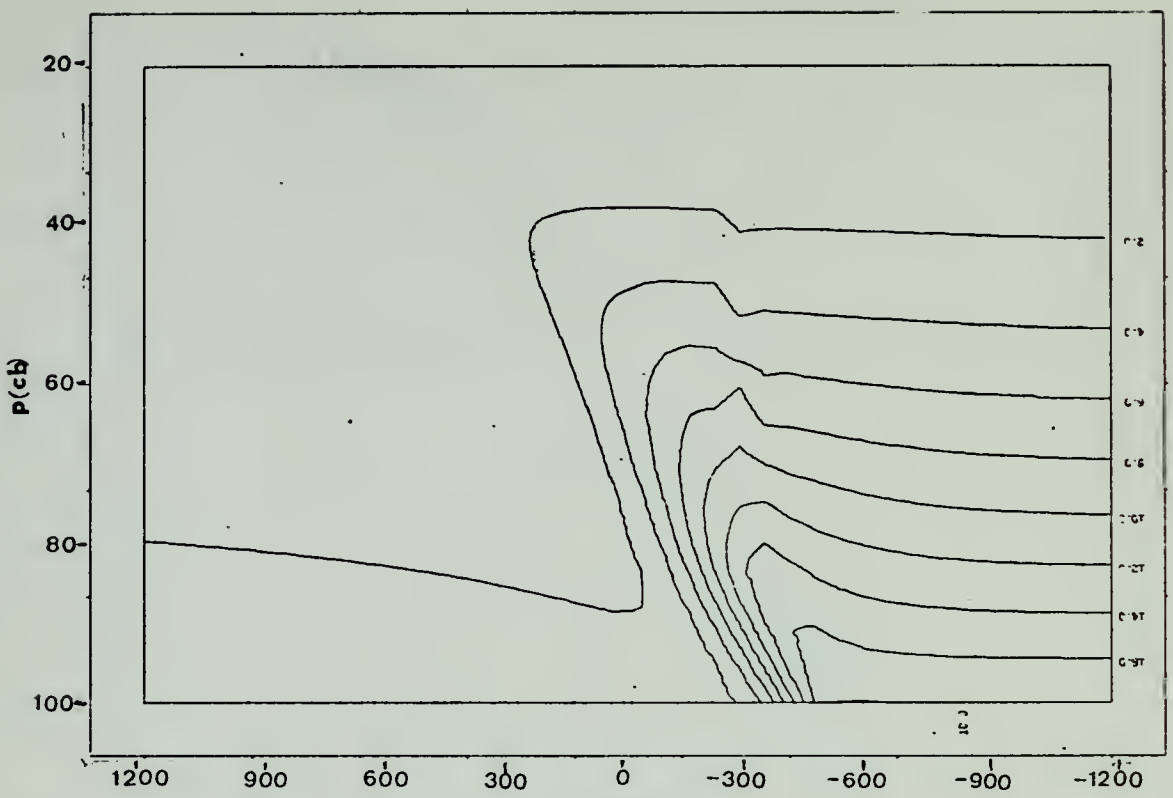

Figure 15. q(g/kg). Exp. 4.

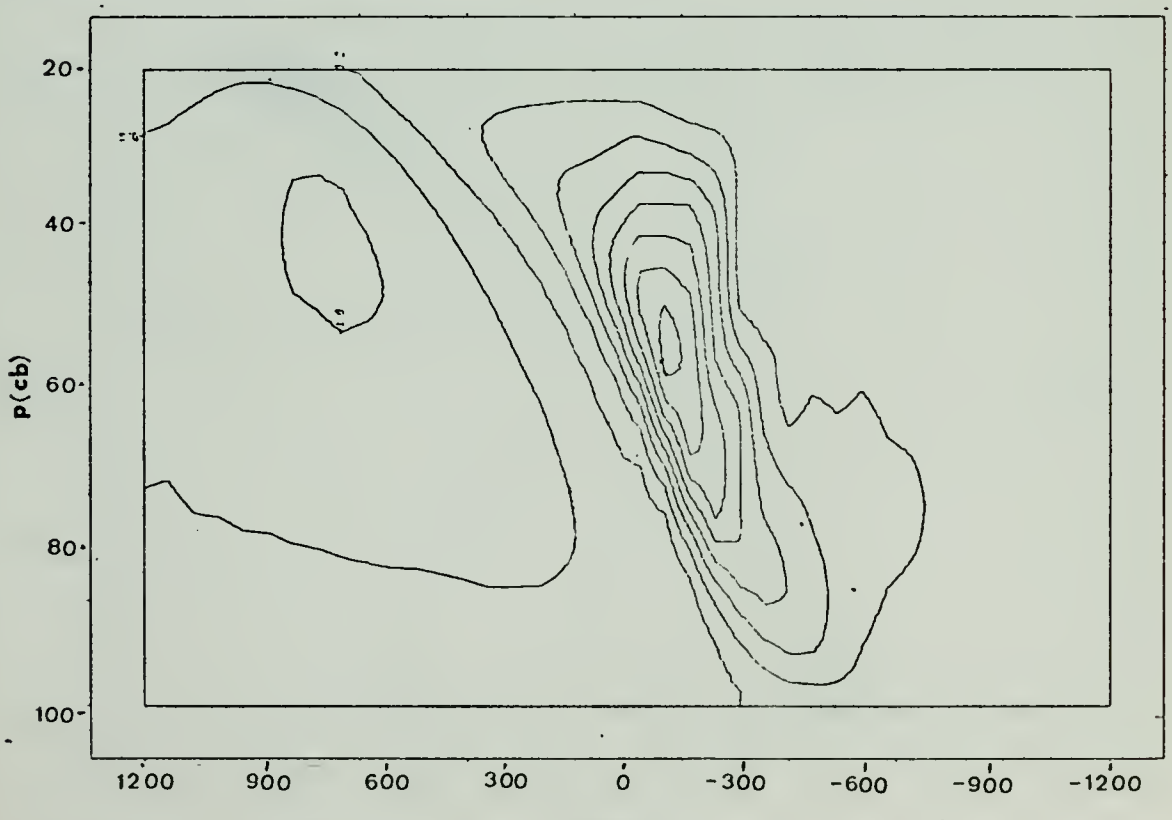

Figure 16. w(x10^{-3}mb/sec). Exp.4.

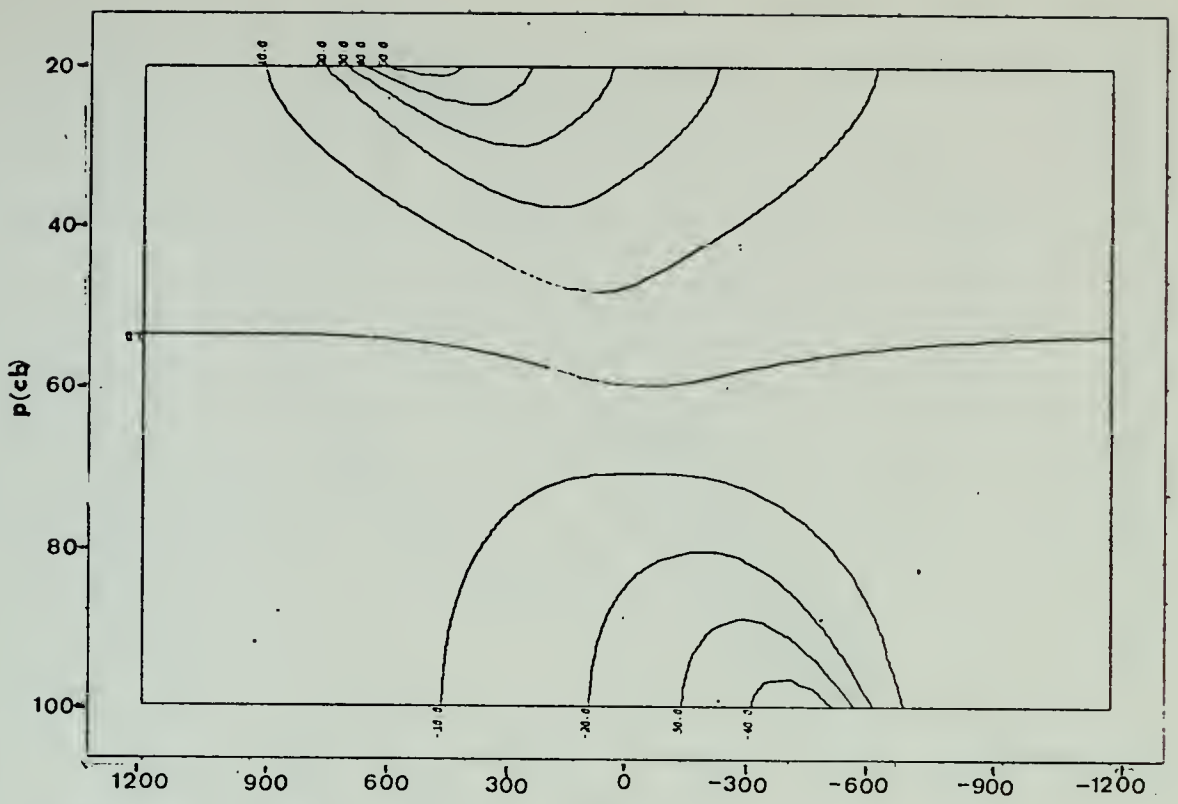

Figure 17. u(m/sec). Exp. 5.

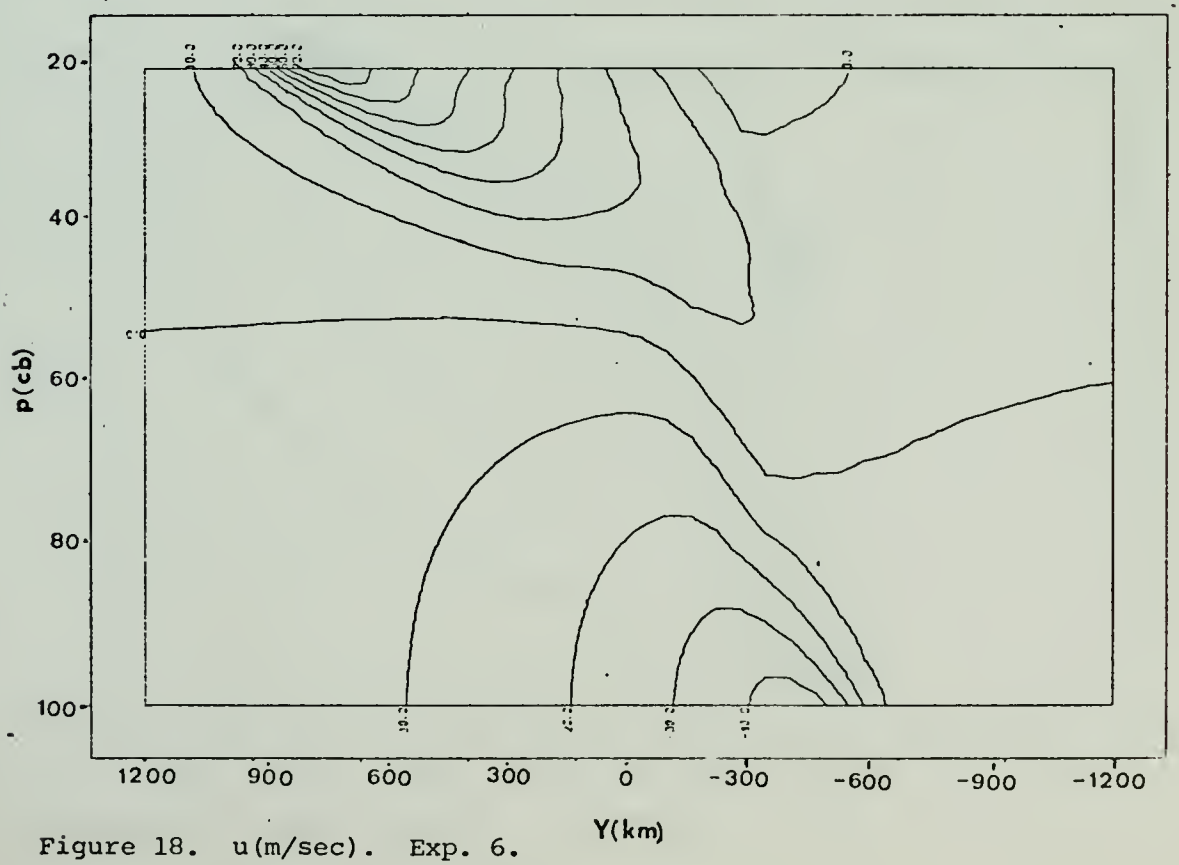

Figure 18. u(m/sec). Exp. 6.

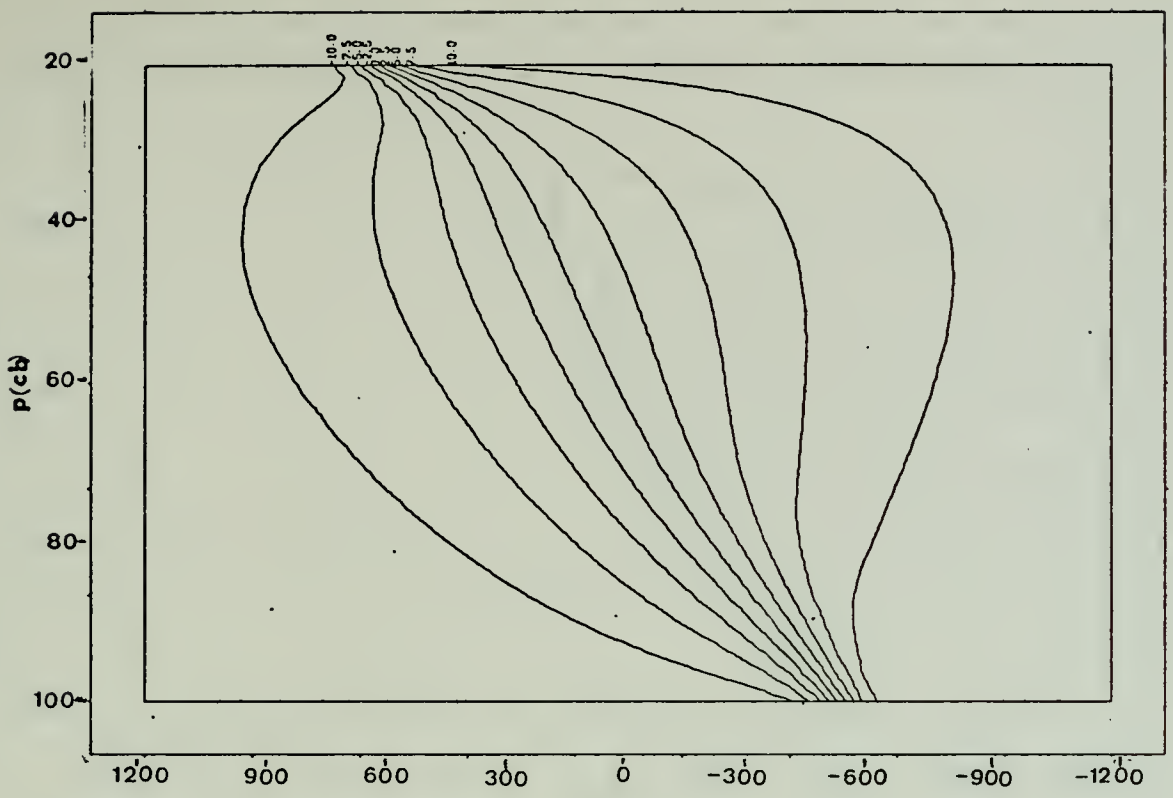

Figure 19. θ'(°K). Exp. 5.

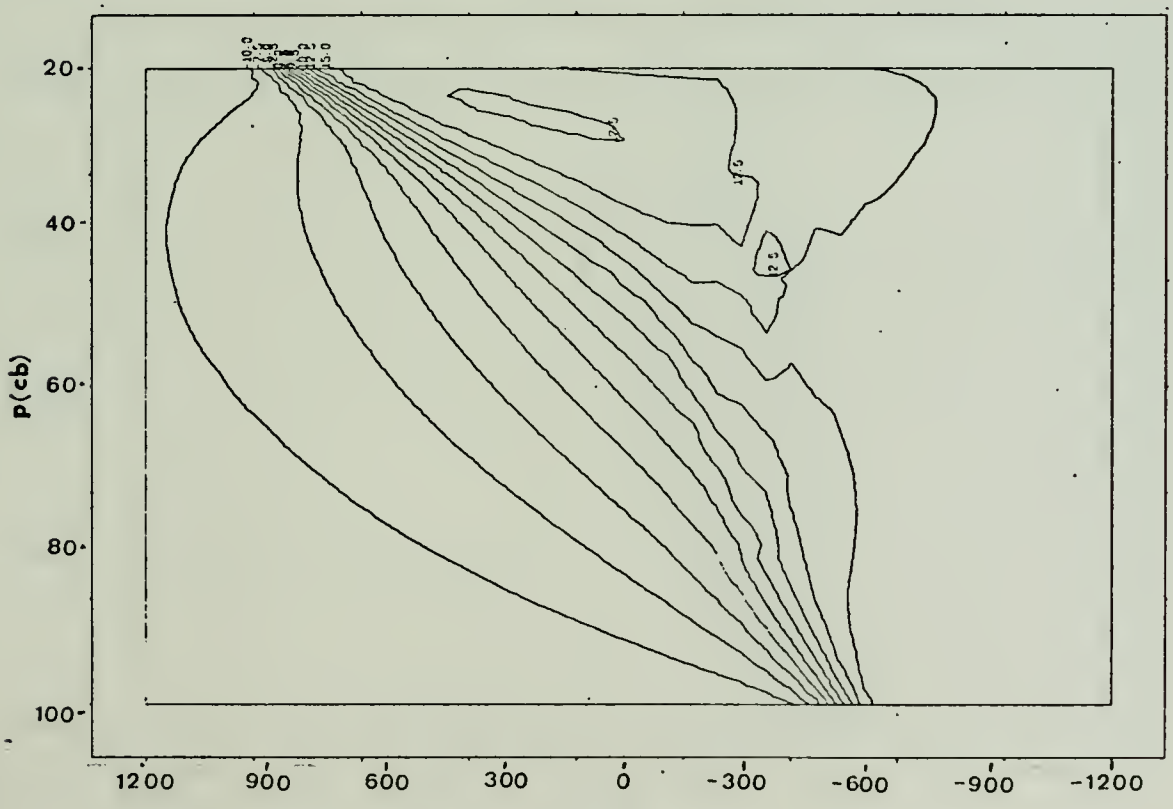

Figure 20. θ'(°K). Exp. 6.

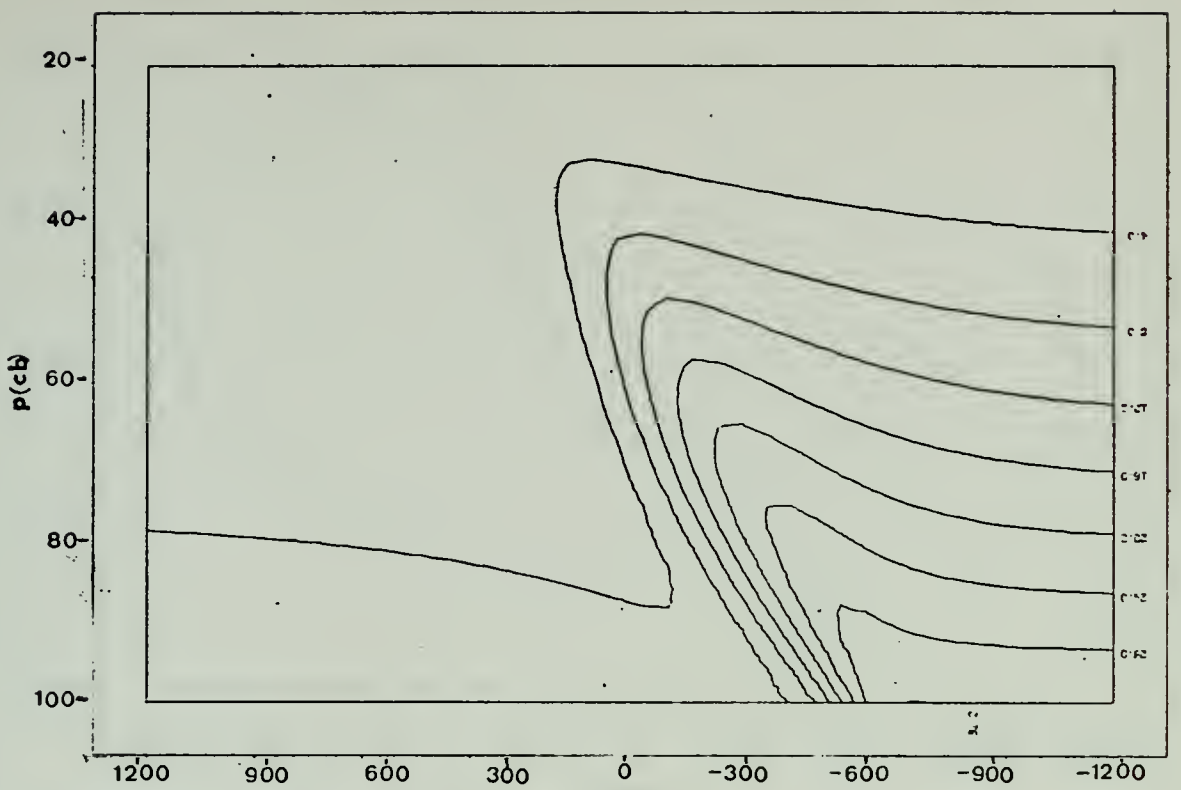

Figure 21. q(g/kg). Exp. 5.

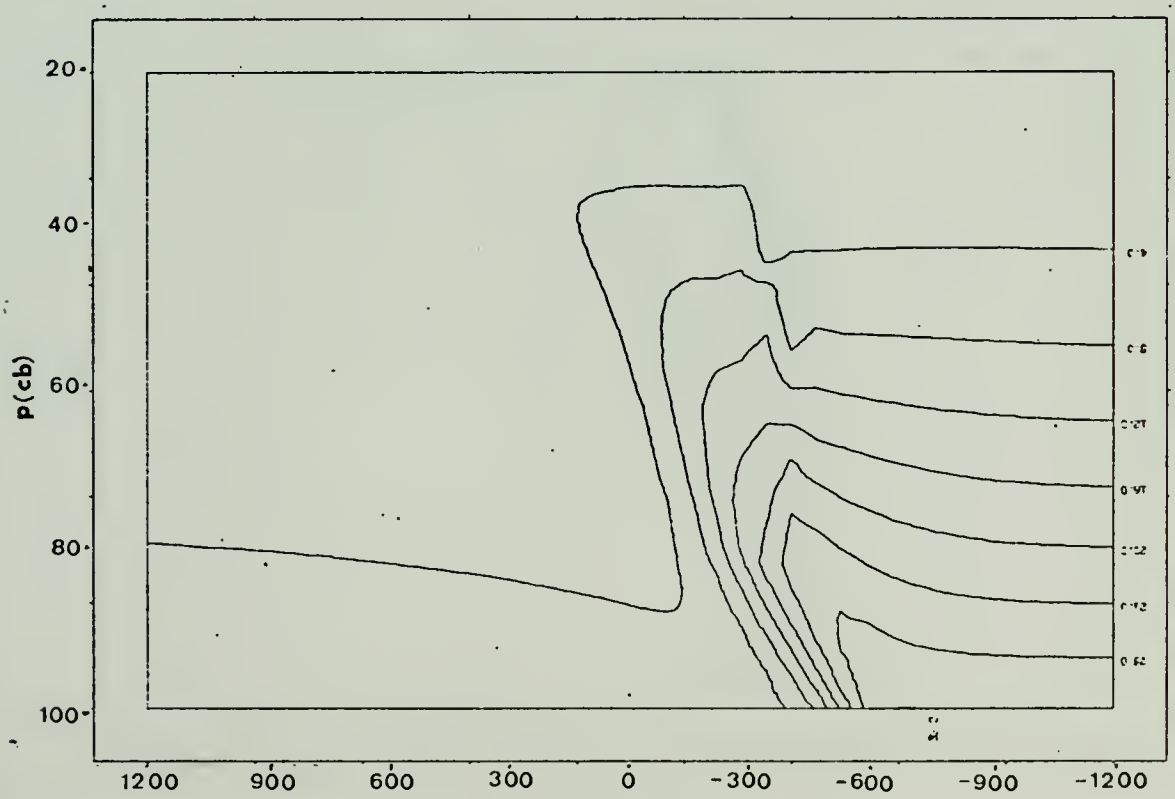

Figure 22. q(g/kg). Exp. 6.

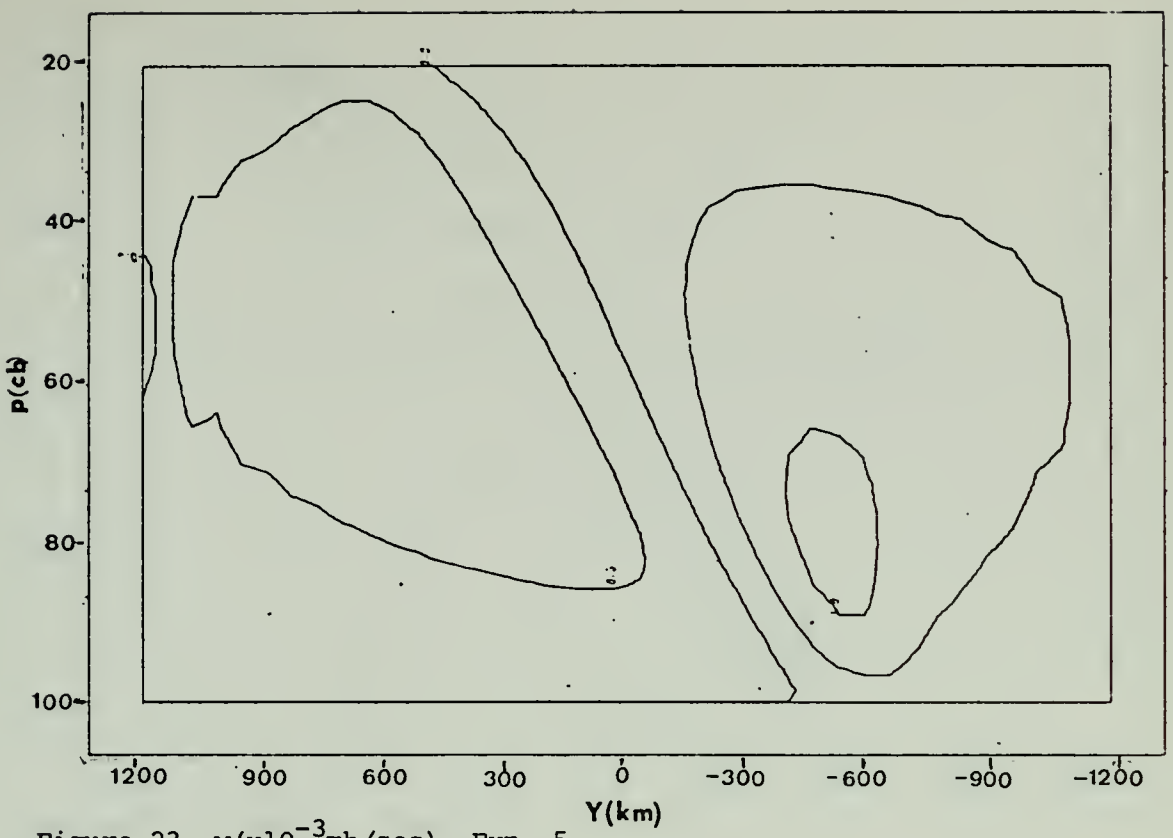

Figure 23. w(x10^{-3}mb/sec). Exp. 5.

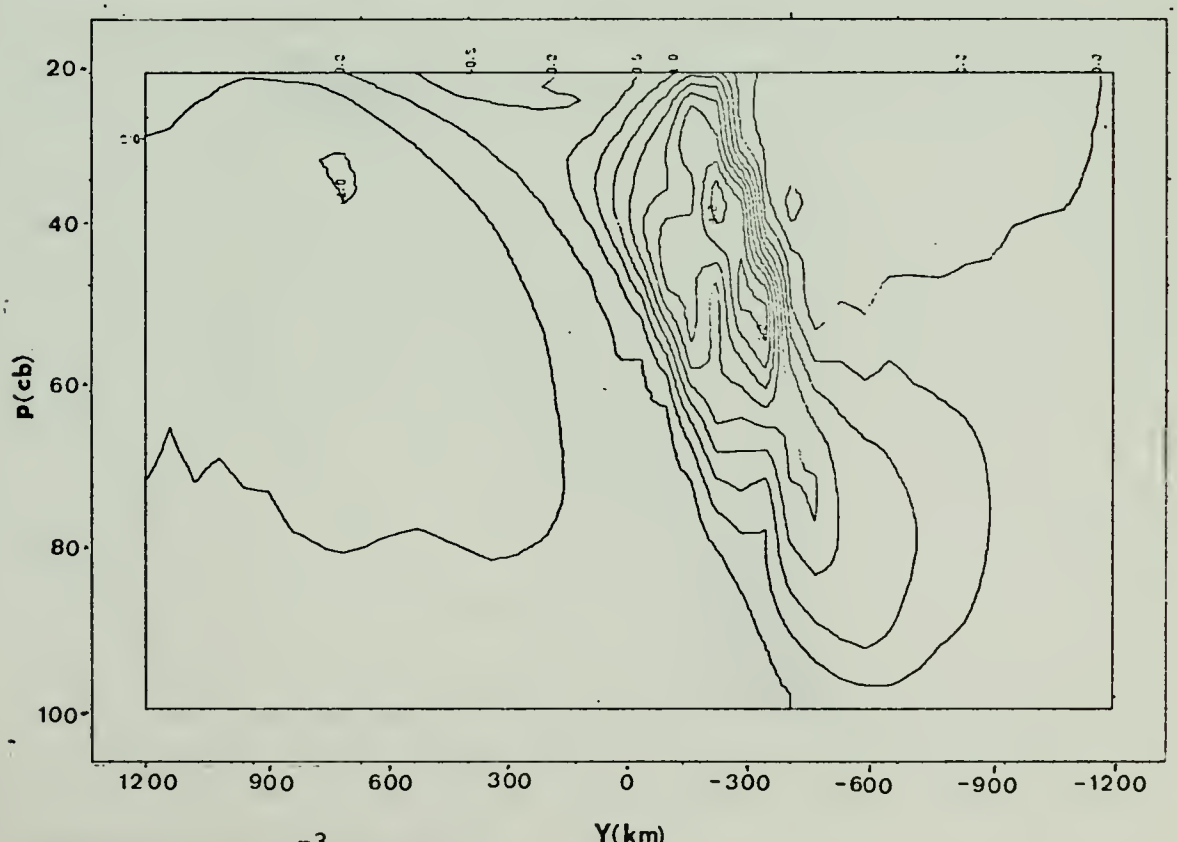

Figure 24. w(x10^{-3}mb/sec). Exp. 6.

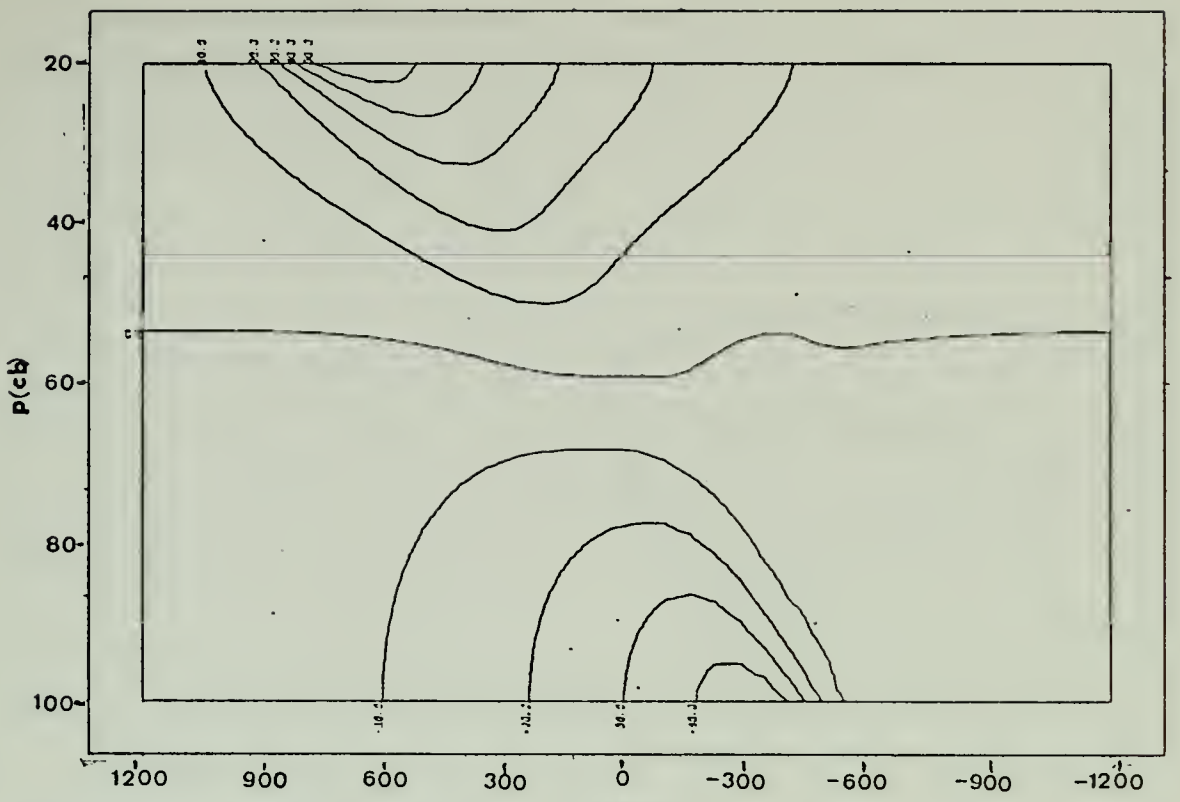

Figure 25. u(m/sec). Exp. 11.

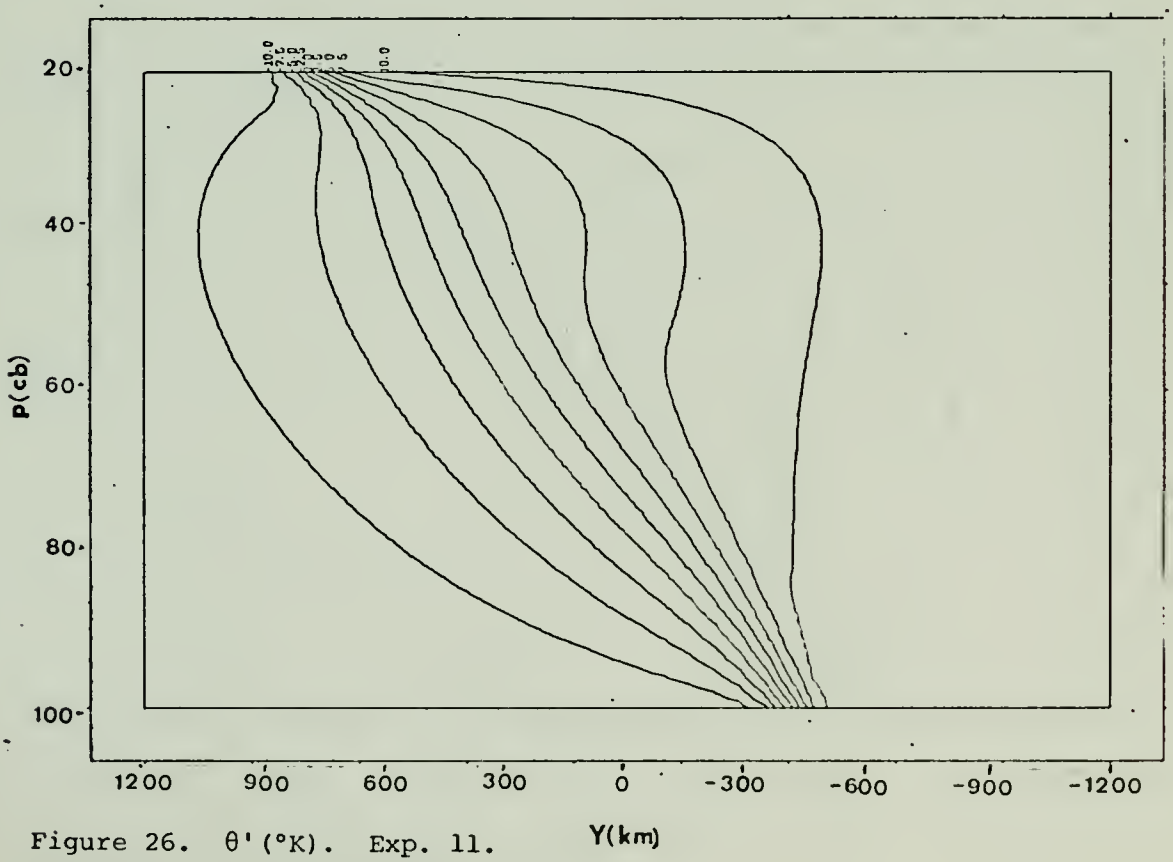

Figure 26. θ'(°K). Exp. 11.

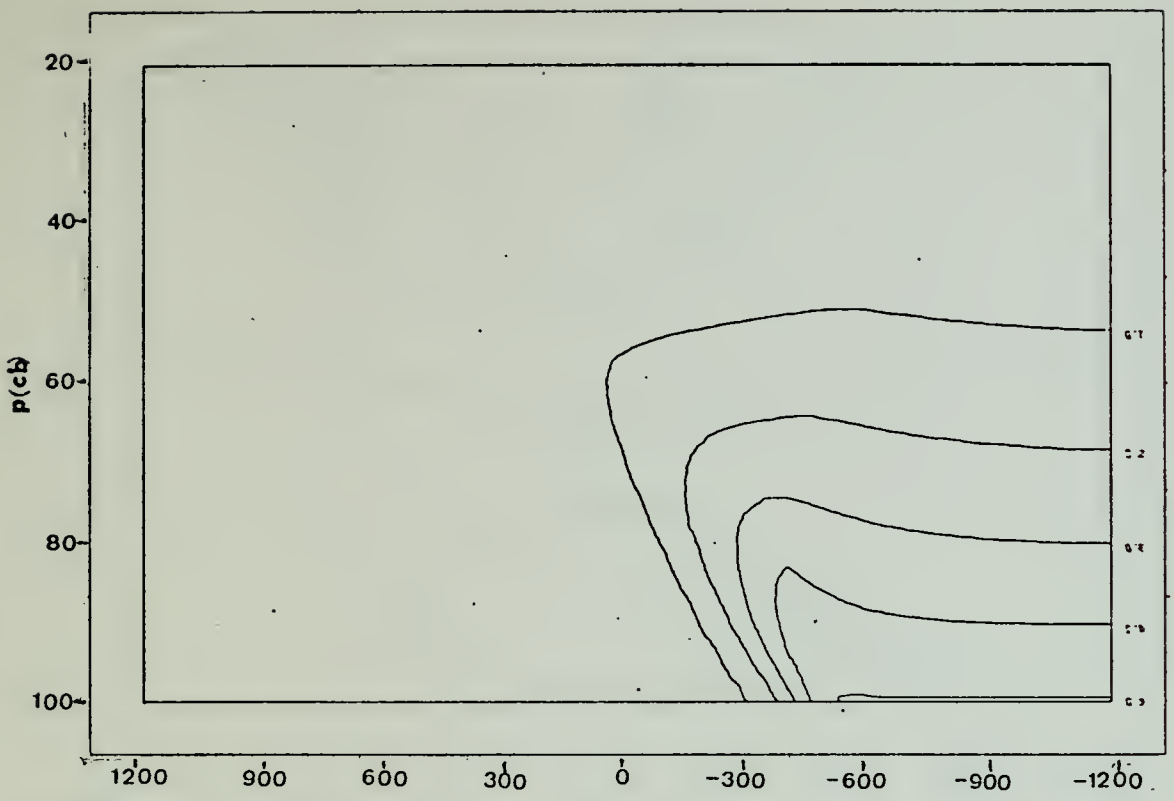

Figure 27. q(g/kg). Exp. 11.

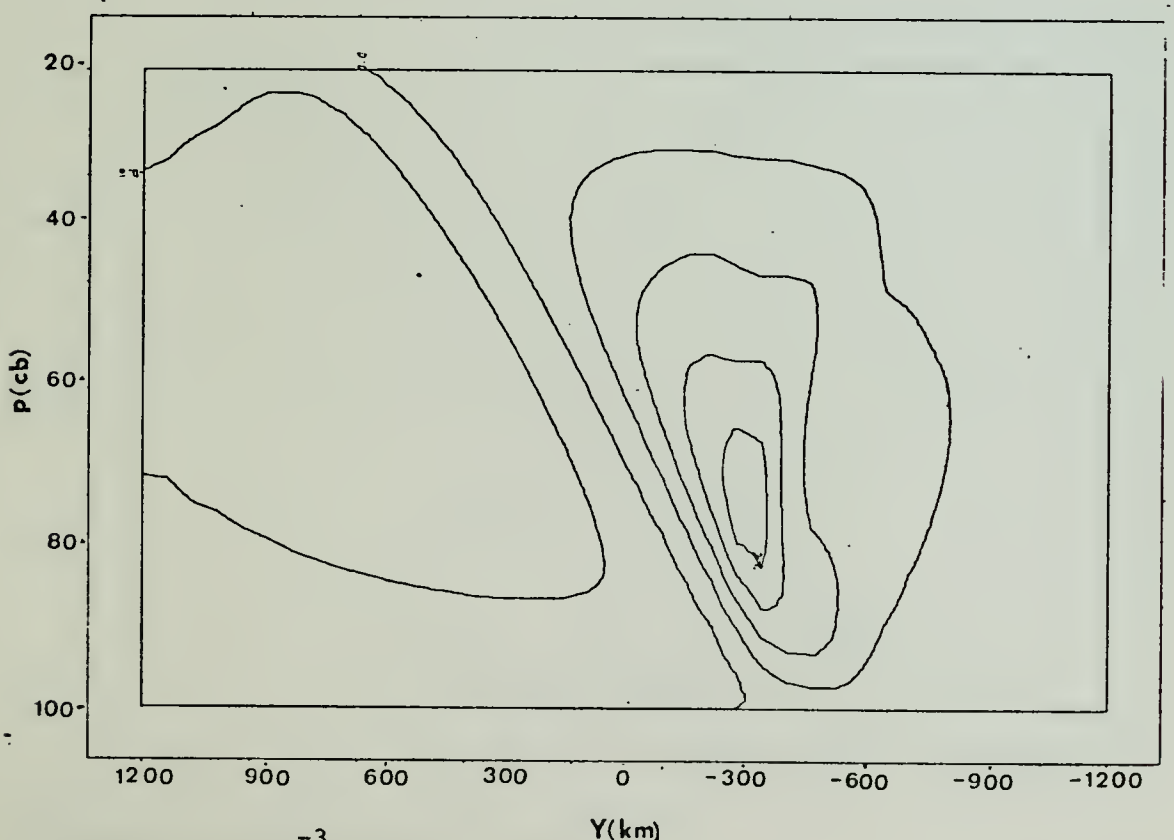

Figure 28. w(x10^{-3}mb/sec). Exp. 11.

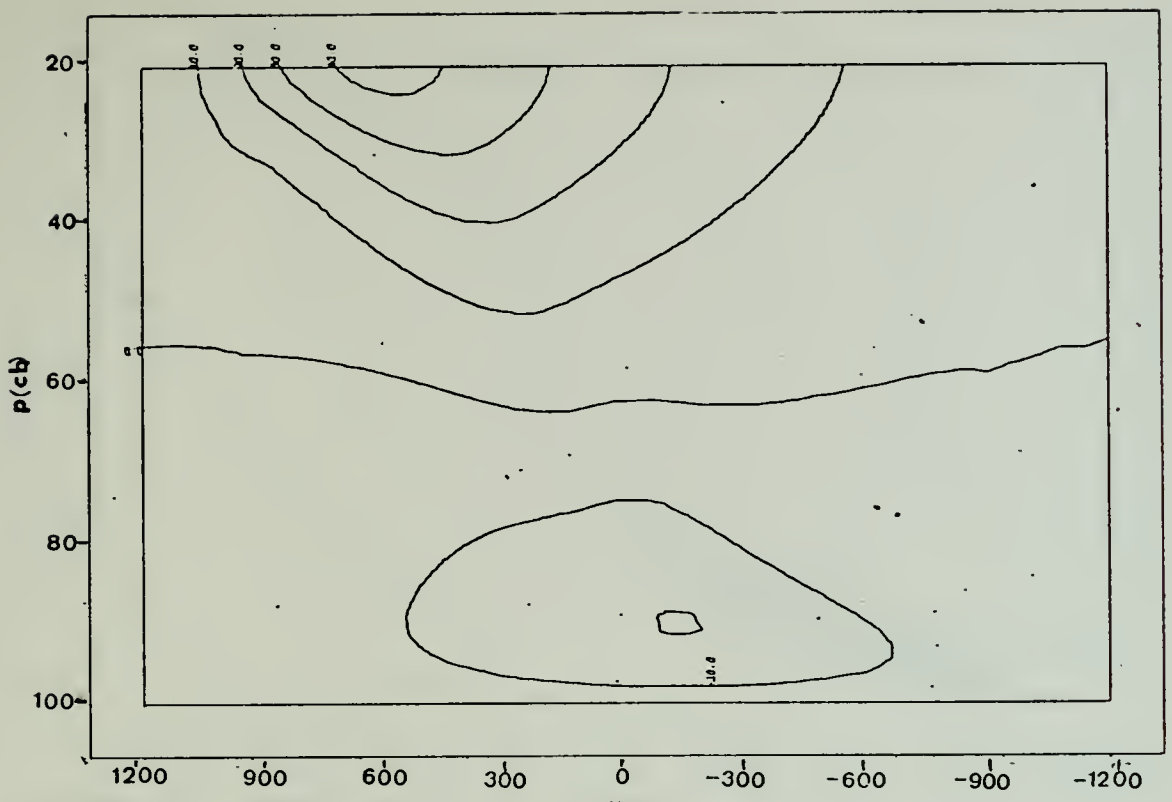

Figure 29. u(m/sec). Exp. 12.

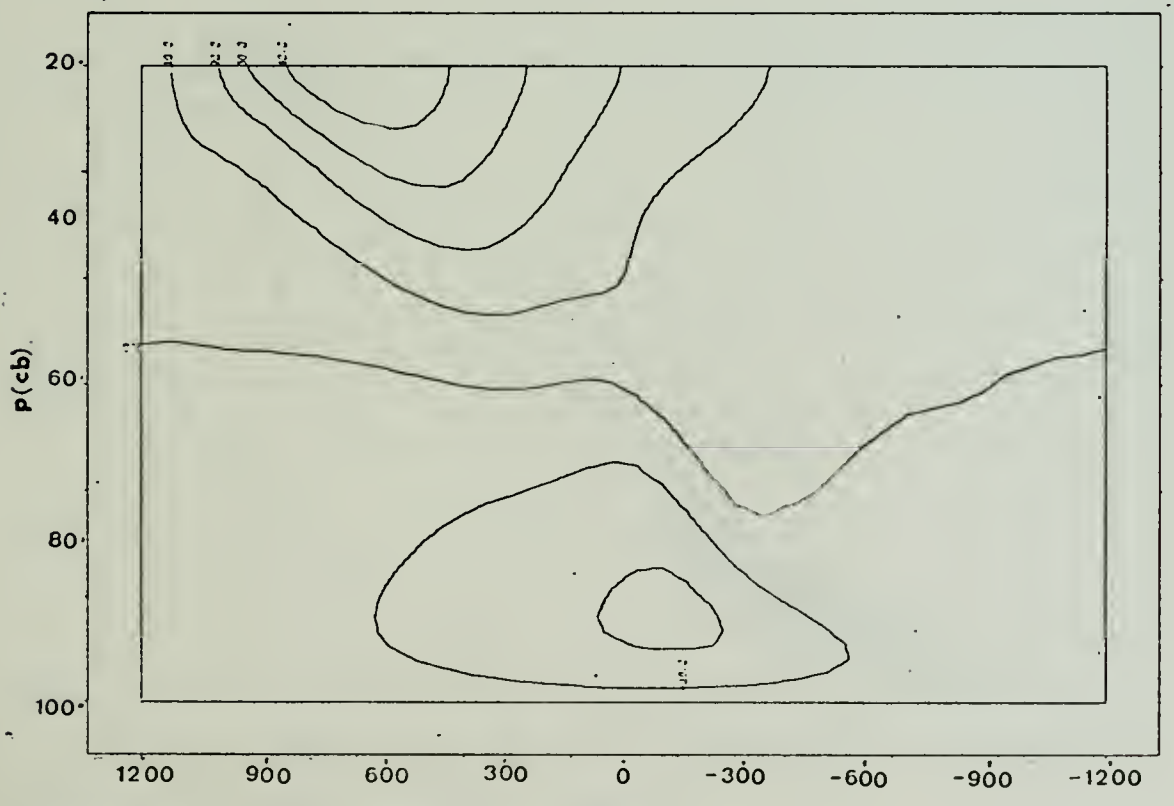

Figure 30. u(m/sec). Exp. 13.

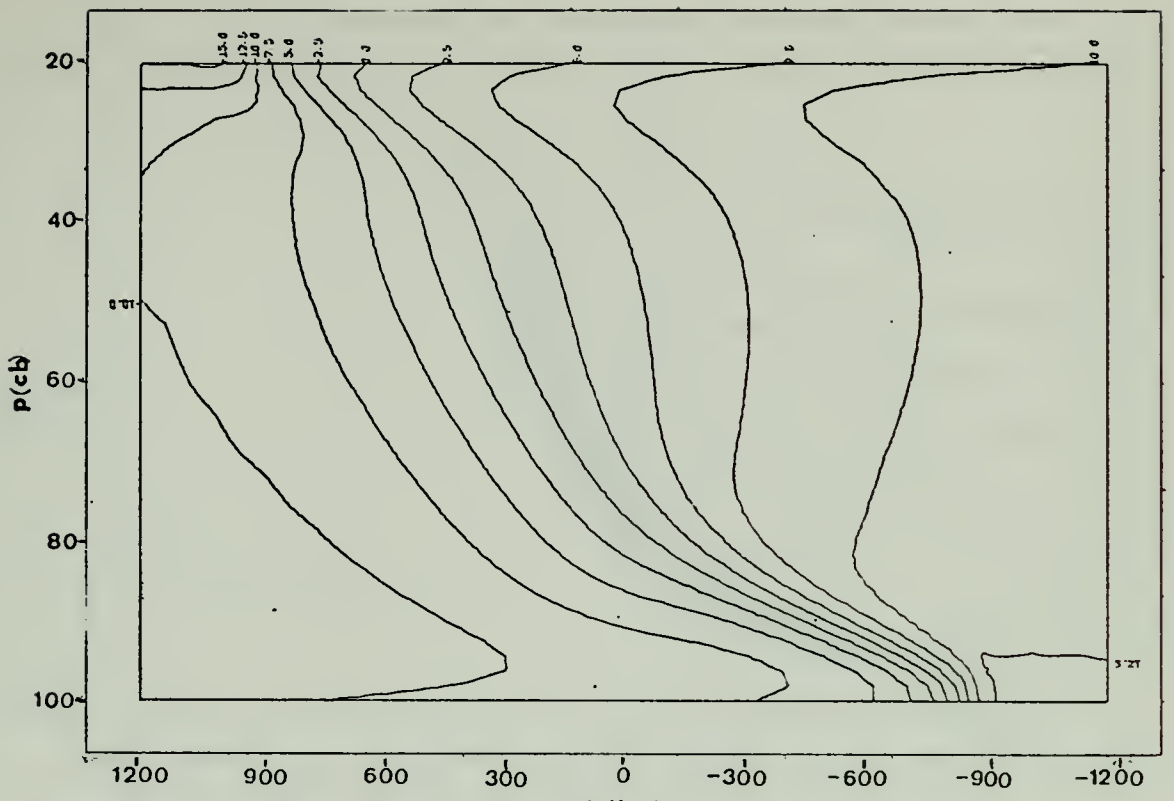

Figure 31. θ'(°K). Exp. 12.

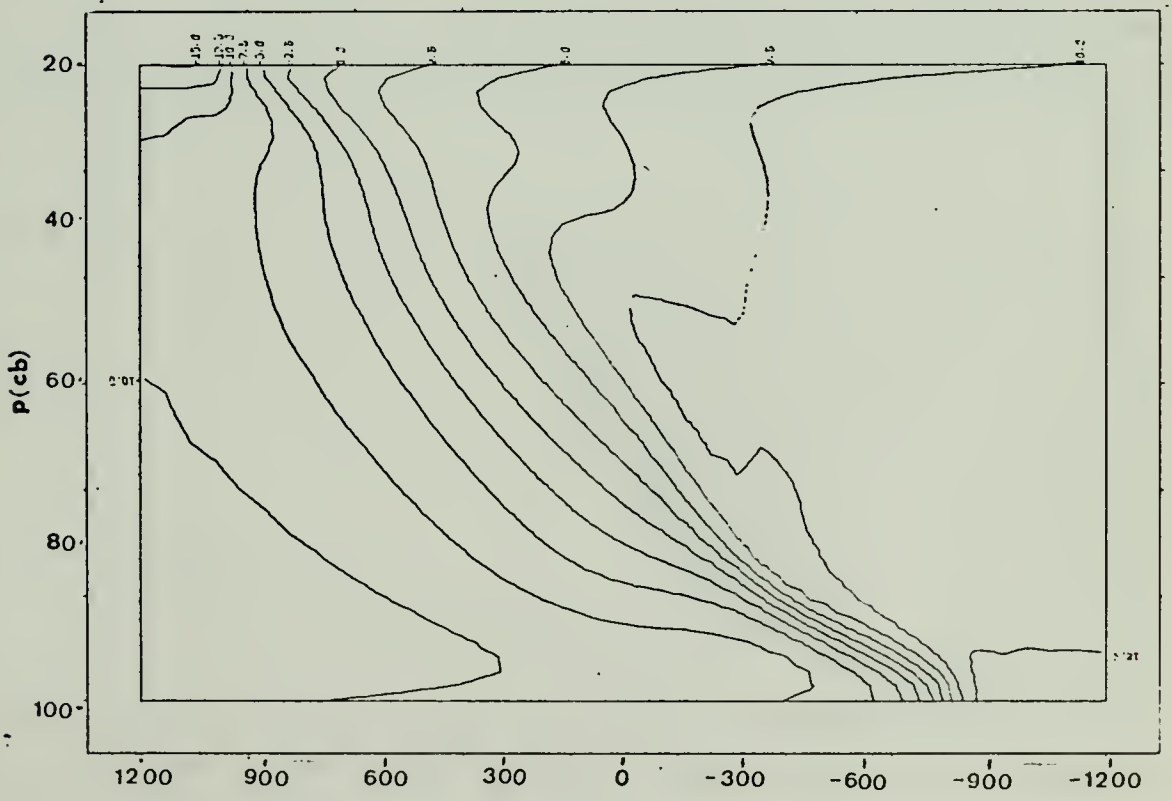

Figure 32. θ'(°K). Exp. 13.

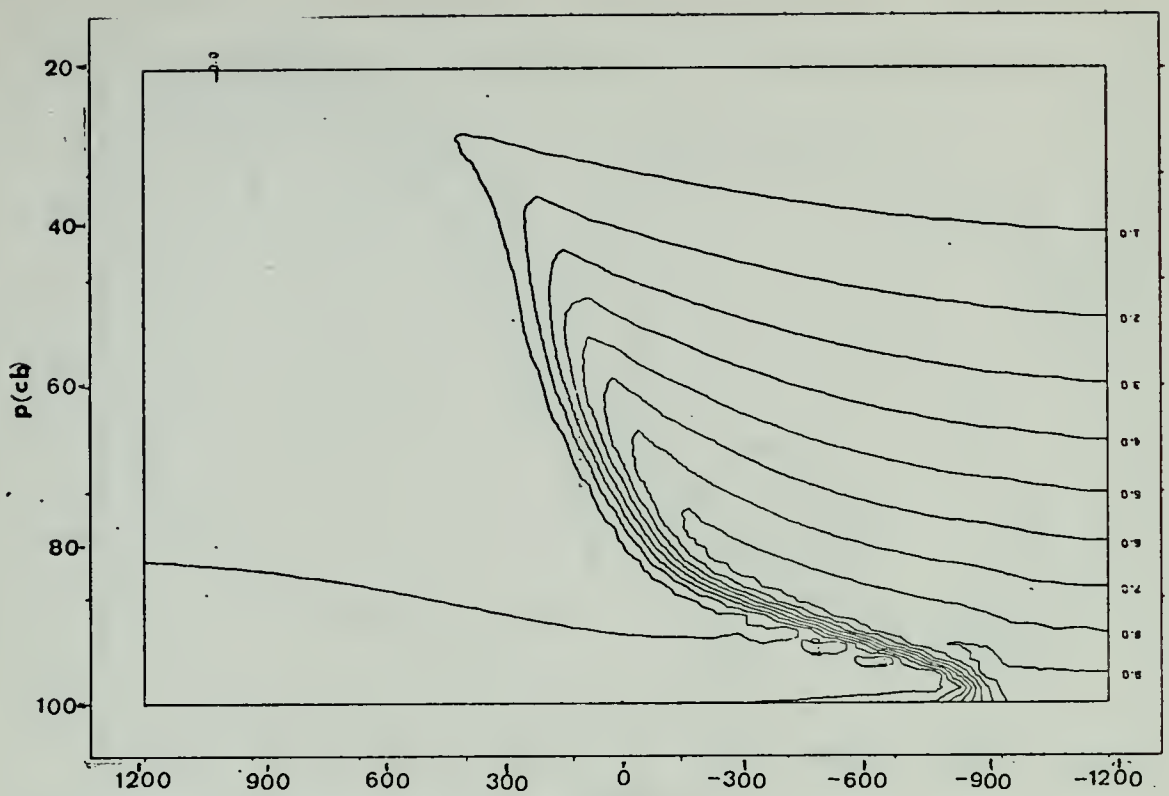

Figure 33. q(g/kg). Exp. 12.

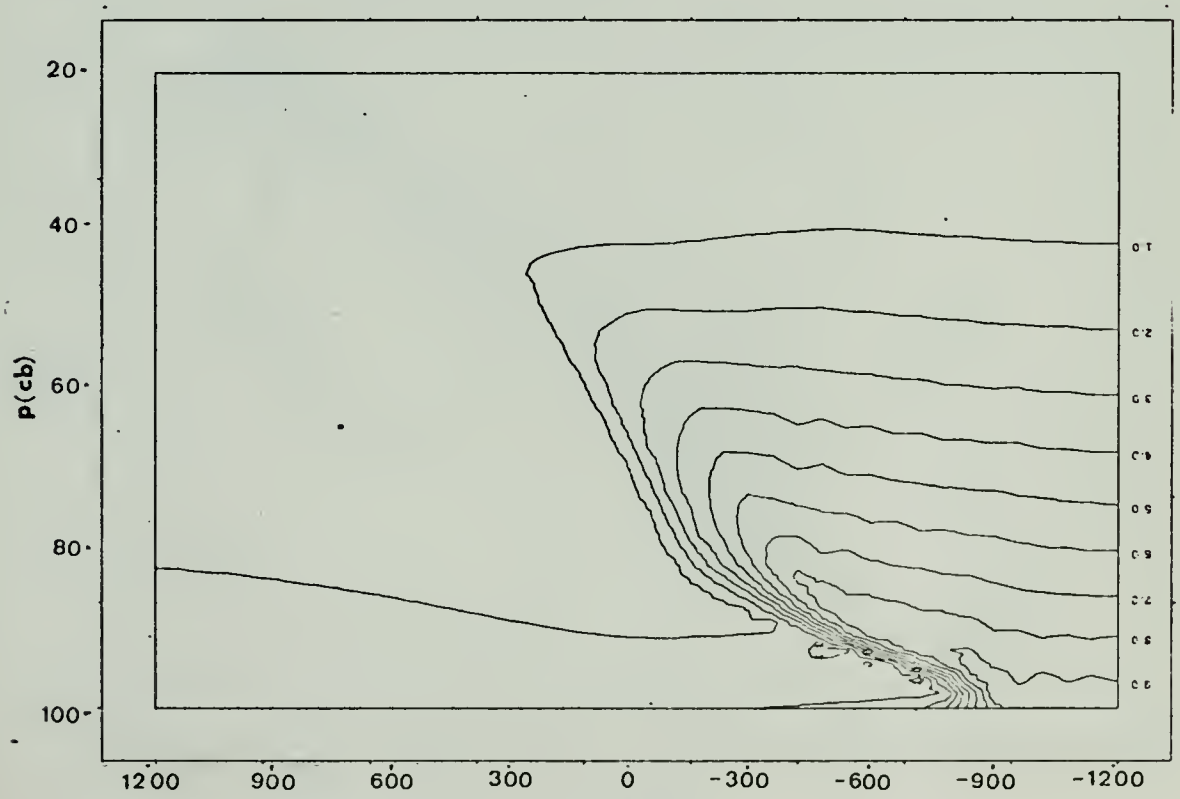

Figure 34. q(g/kg). Exp. 13.

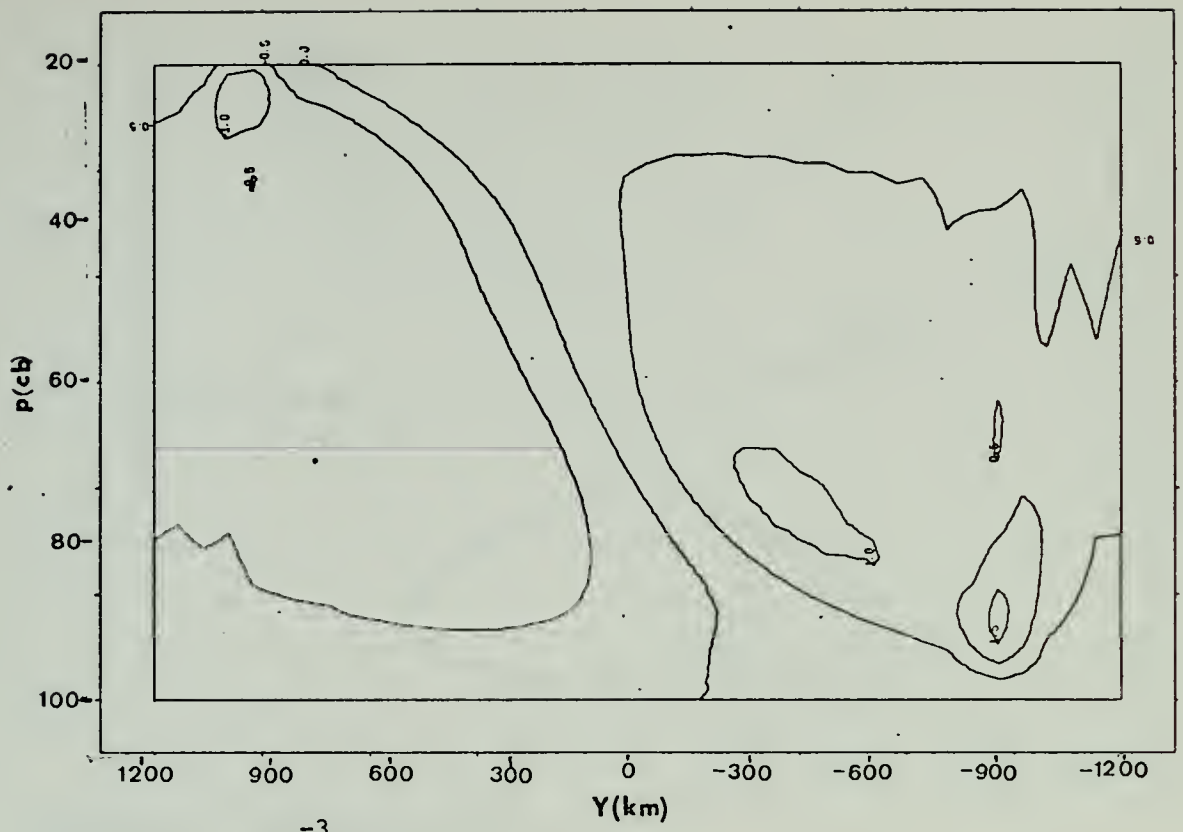

Figure 35. w(x10^{-3}mb/sec). Exp. 12.

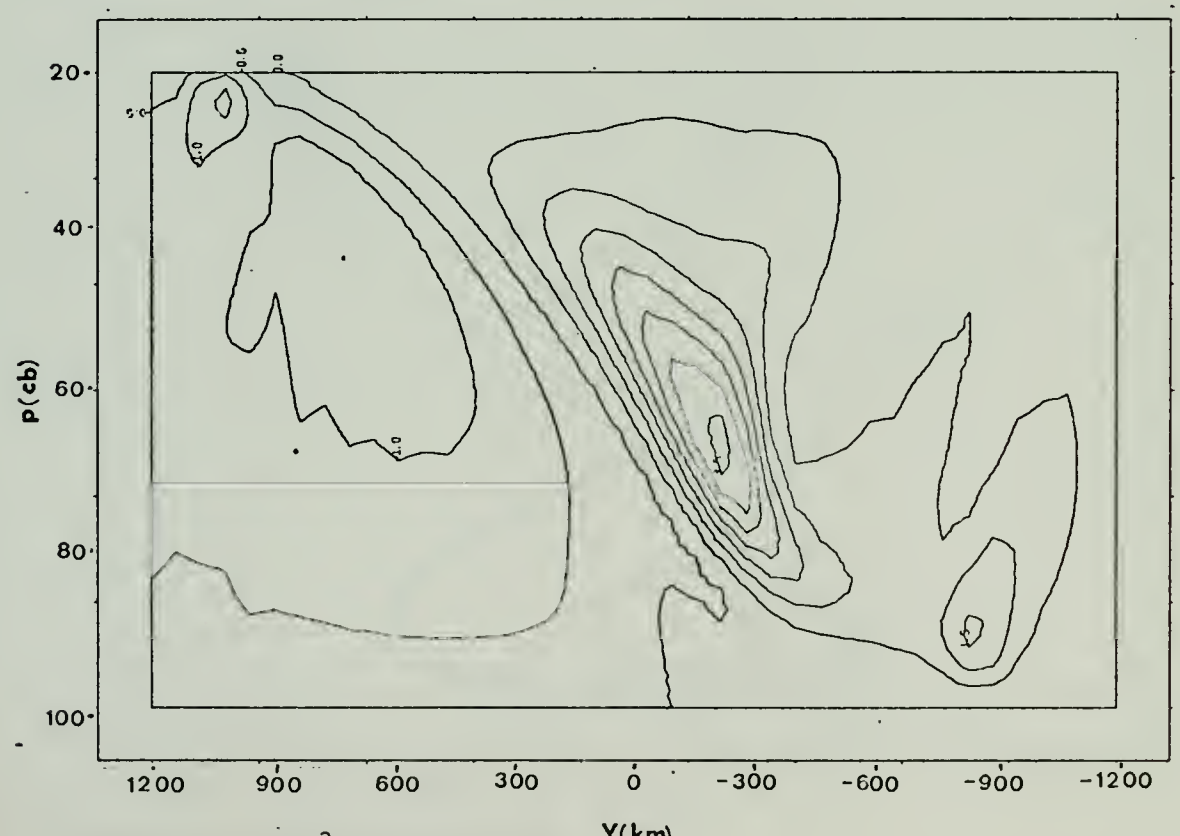

Figure 36. w(x10^{-3}mb/sec). Exp. 13.

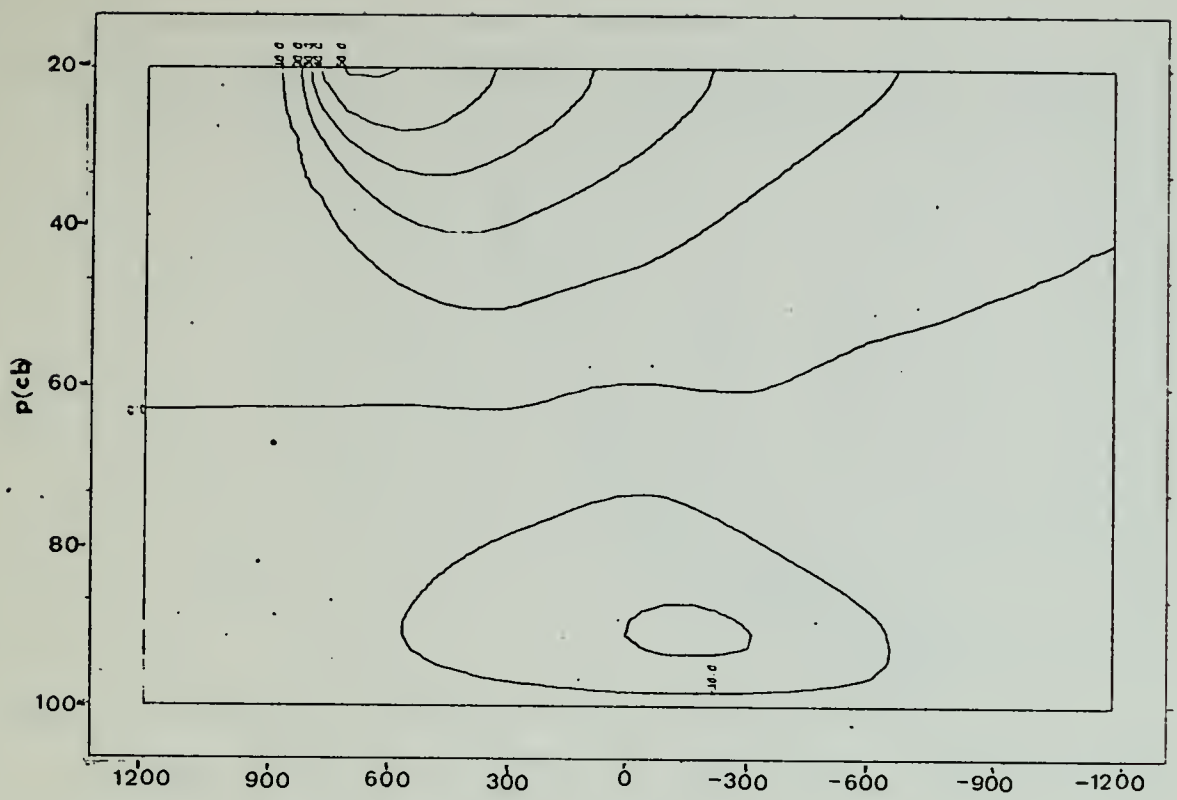

Figure 37. u(m/sec). Exp. 17.

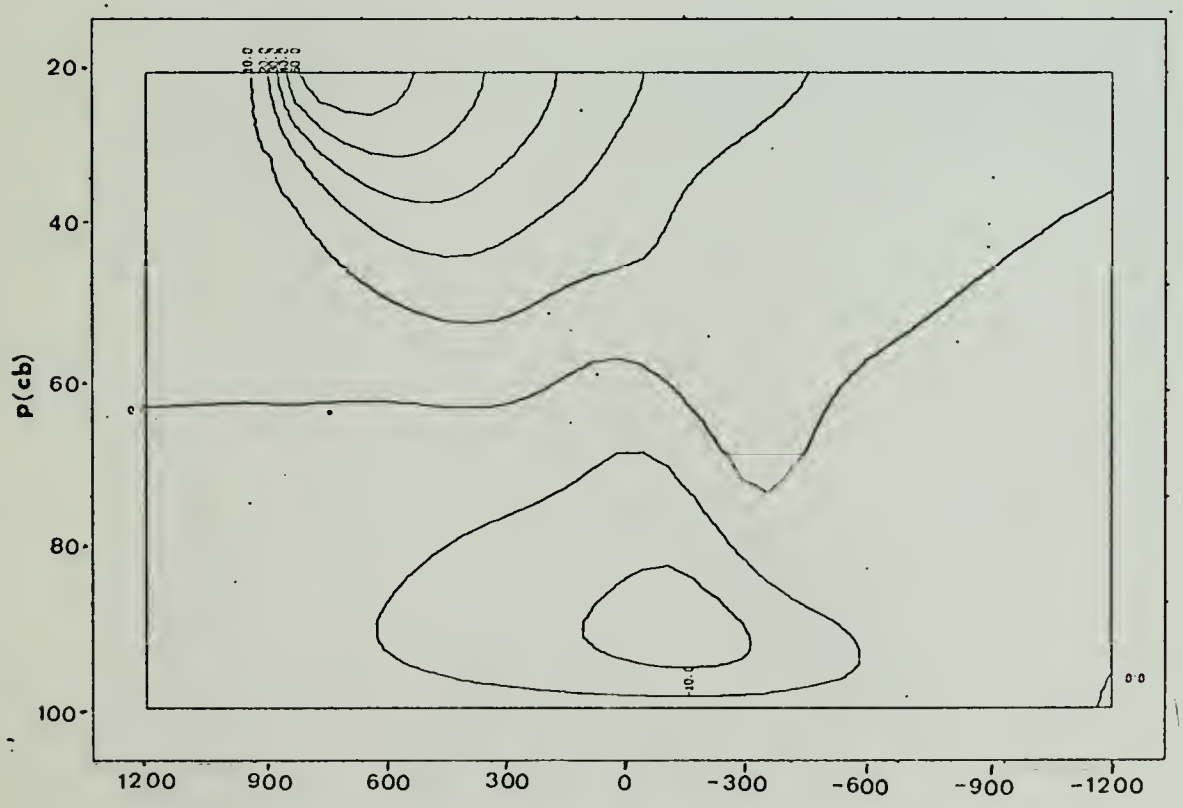

Figure 38. u(m/sec). Exp. 18.

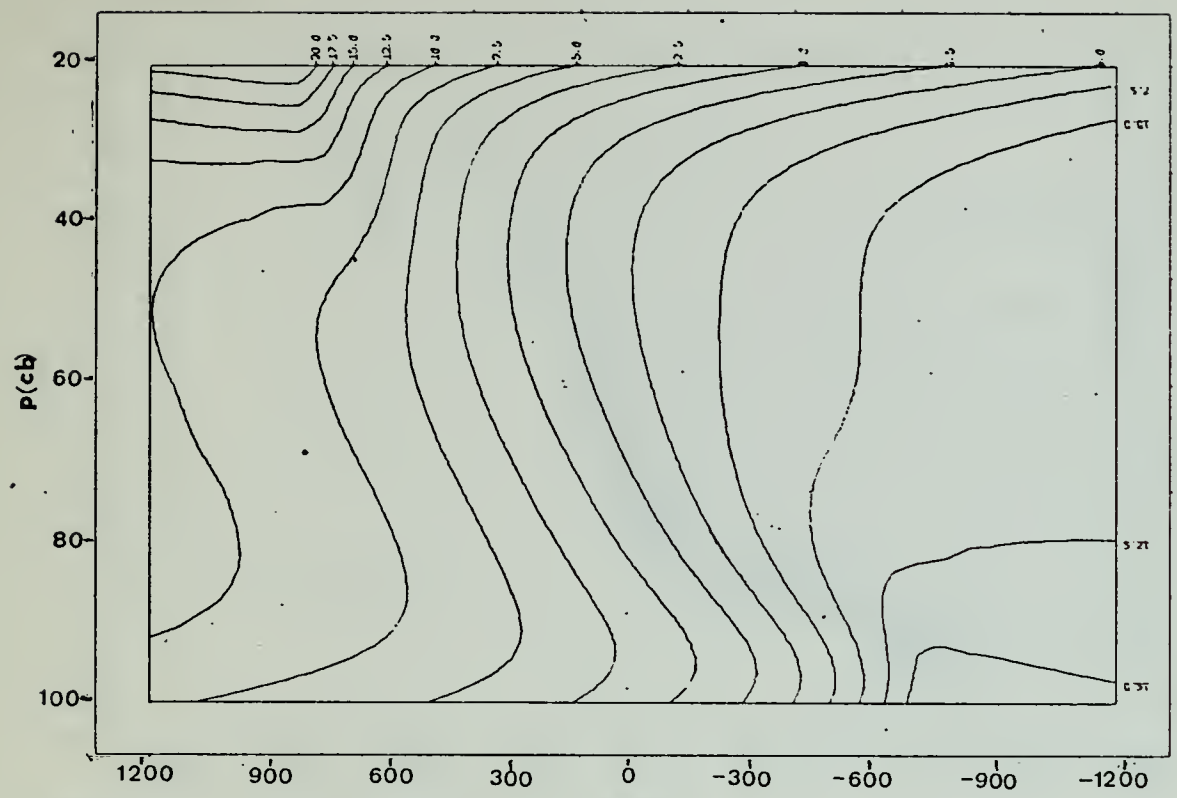

Figure 39. θ'(°K). Exp. 17.

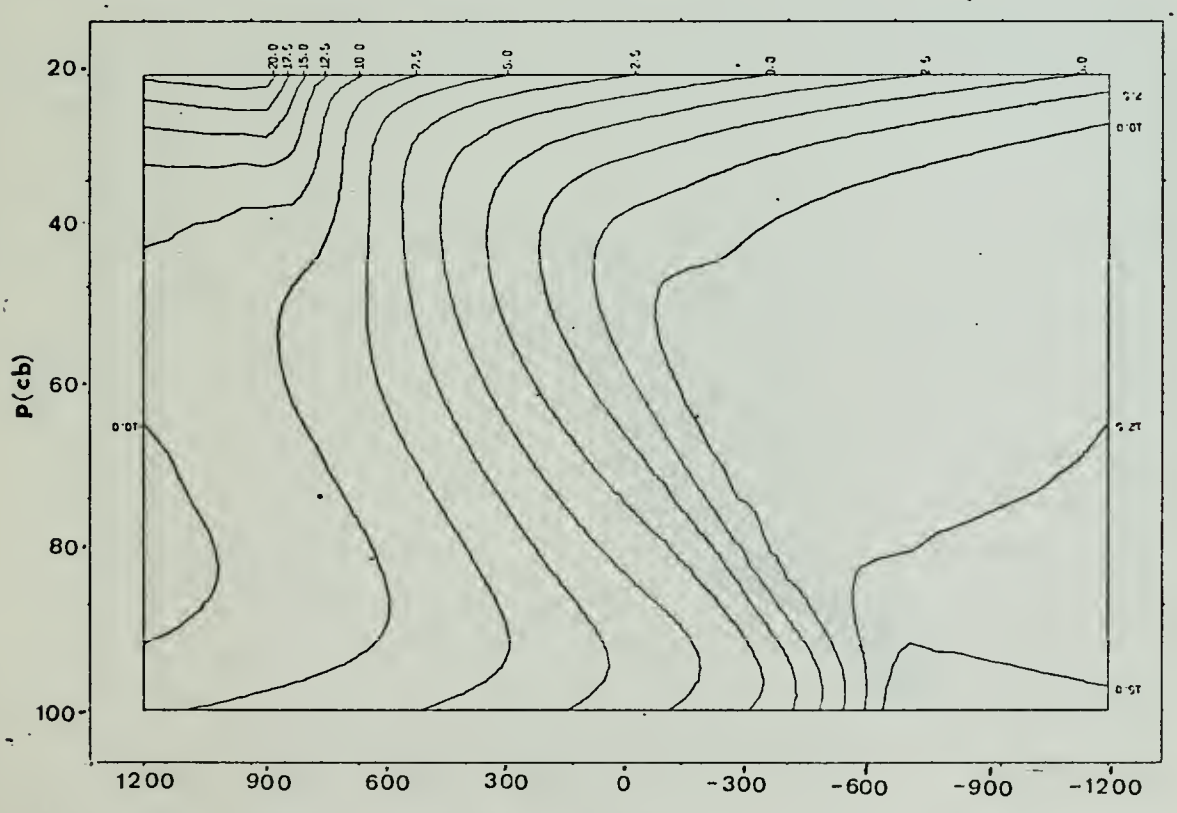

Figure 40. θ'(°K). Exp. 18.

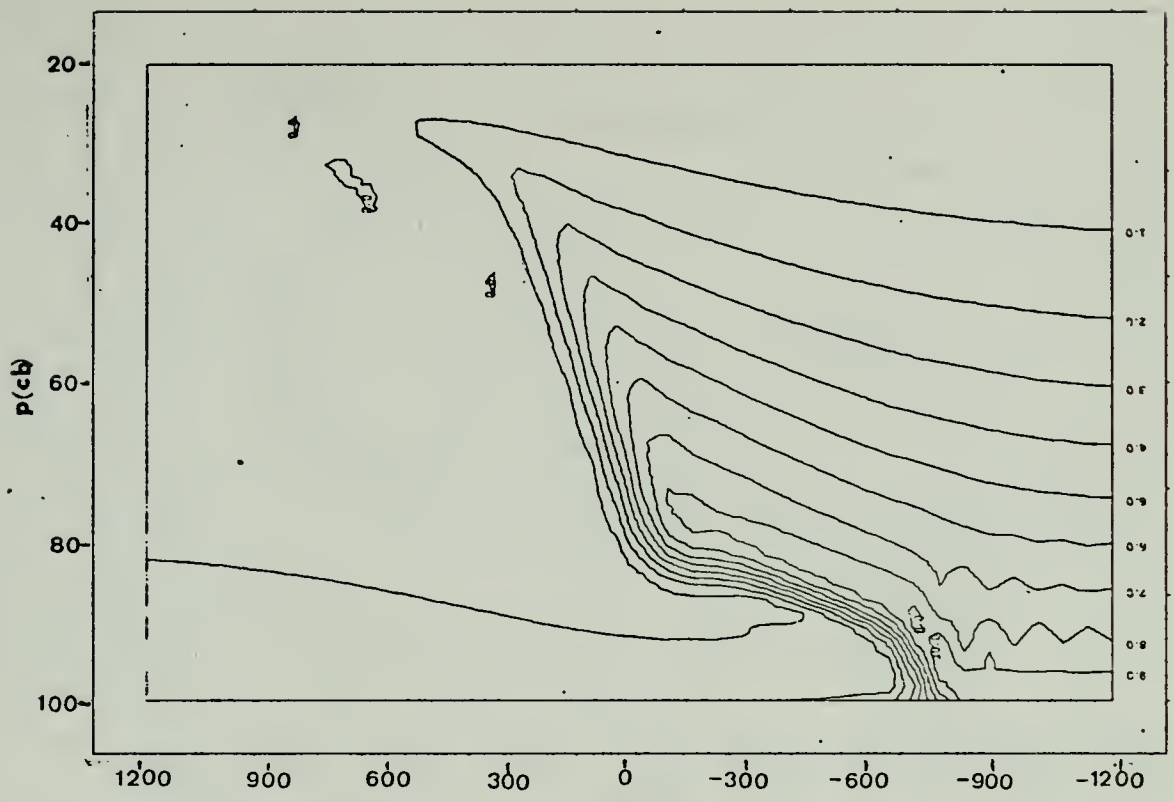

Figure 41. q(g/kg). Exp. 17.

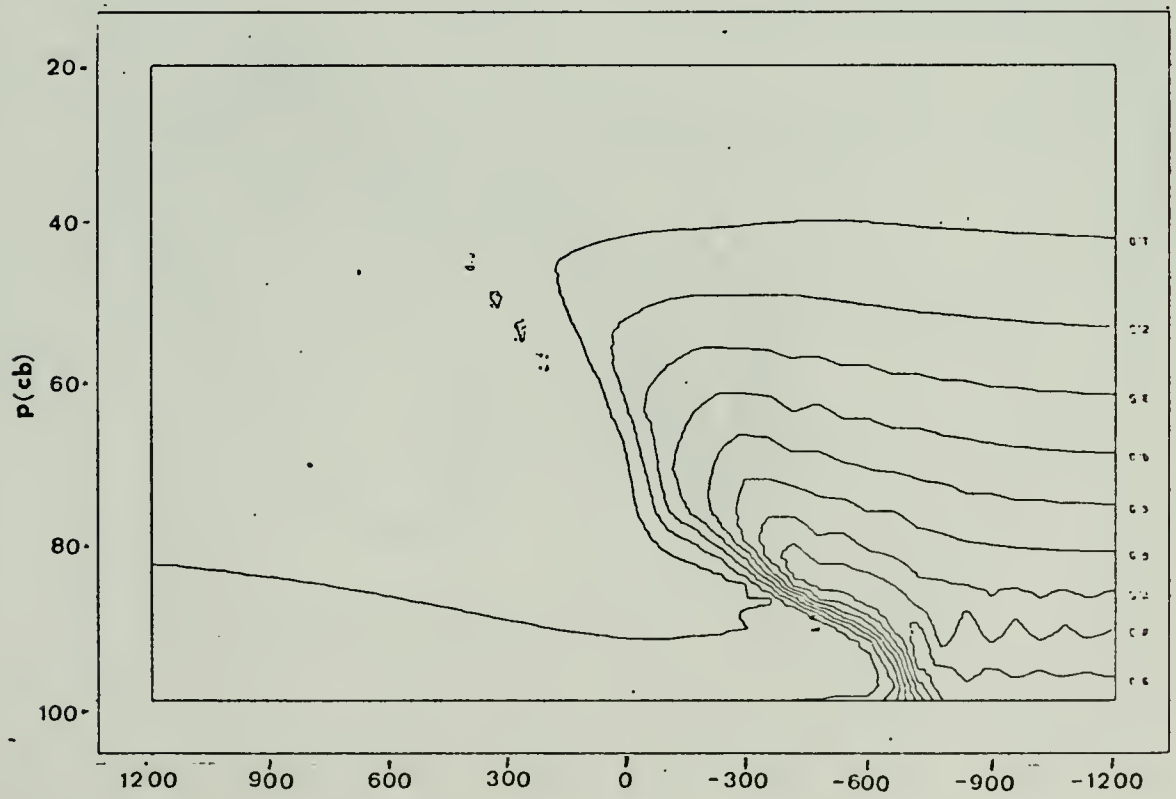

Figure 42. q(g/kg). Exp. 18.

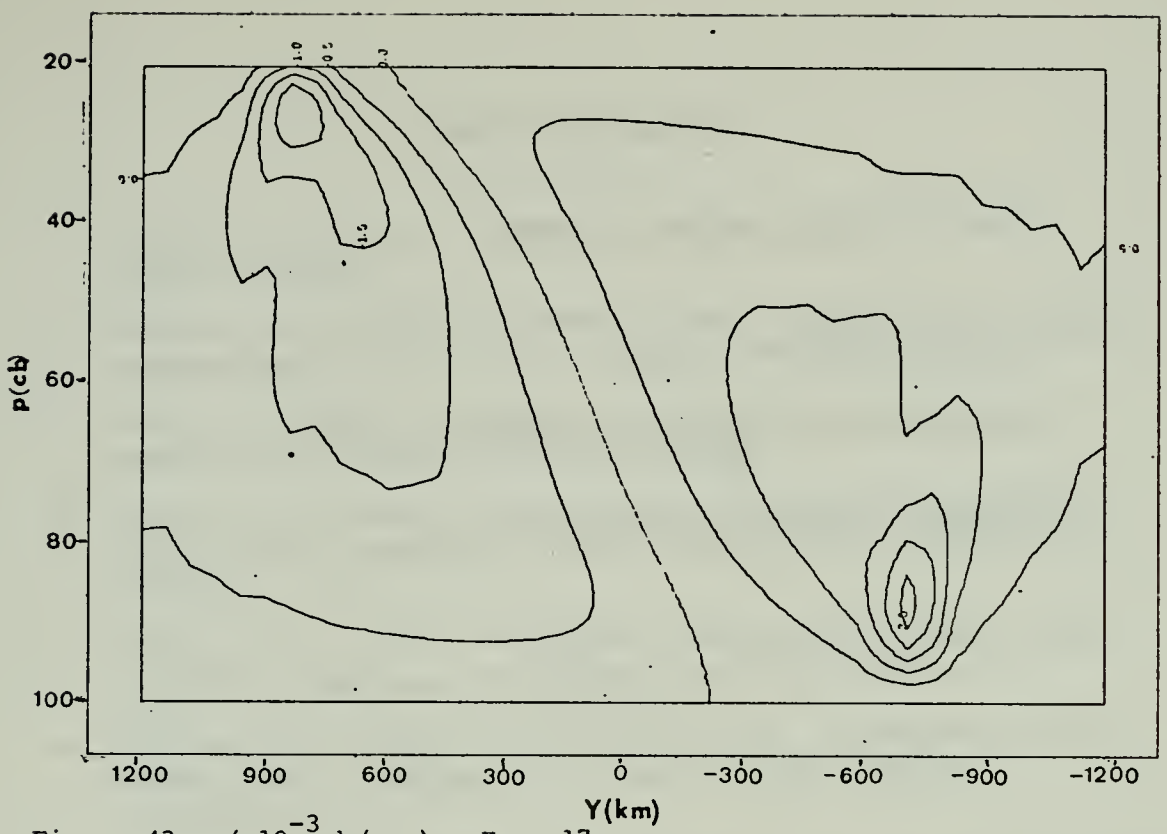

Figure 43. w(x10^{-3}mb/sec). Exp. 17.

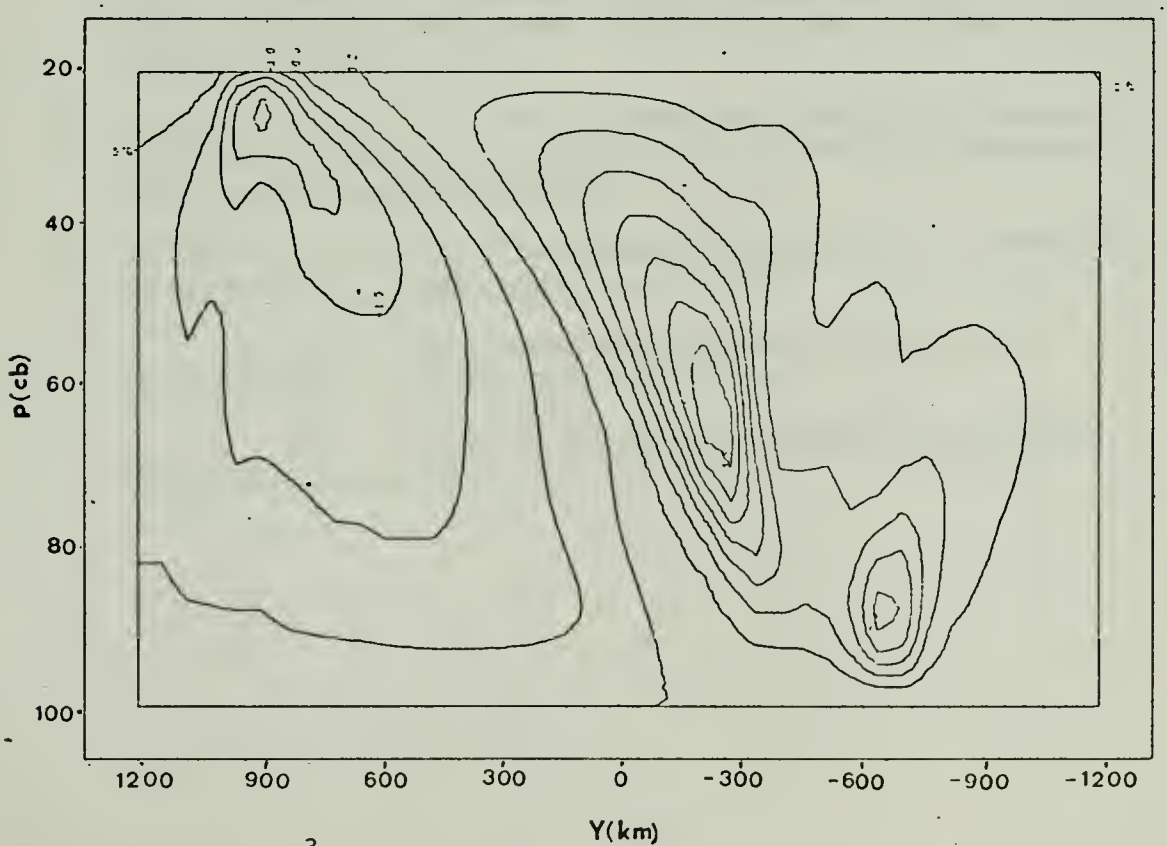

Figure 44. w(x10^{-3}mb/sec). Exp. 18.

LIST OF REFERENCES

1. Haltiner, G. J., ____: Numerical Weather Prediction Notes. Unpublished notes.

2. Haltiner, G. J., and F. L. Martin, 1957: Dynamical and Physical Meteorology, McGraw Hill Book Company, New York, 470 pp.

3. Hess, S. L., 1959: Introduction to Theoretical Meteorology, Henry Holt and Company, New York, 362 pp.

4. Holton, J. R., 1972: An Introduction to Dynamic Meteorology, International Geophysical series, Academic Press, New York, 16, 319 pp.

5. Hoskins, B. J., 1971: "Atmospheric Frontogenesis Models: Some Solutions." Quart. J. Roy. Meteor. Soc., 97, 139-153.

6. Hoskins, B. J., and F. P. Bretherton, 1972: "Atmospheric Frontogenesis Models: Mathematical Formulation and Solution." J. Atmos. Sci., 29, 11-37.

7. Ogura, Y., and J. G. Charney, 1962: A Numerical Model of Thermal Convection in the Atmosphere. Proc. Int. Symp. on Numer. Weather Predict., Tokyo, 431-452.

8. Platzman, G. W., 1954: "The Computational Stability of Boundary Conditions in Numerical Integration of the Velocity Equation." Arch. Meteor. Geophys. Bioklim., 7, 29-40.

9. Williams, R. T., 1967: "Atmospheric Frontogenesis: A Numerical Experiment." J. Atmos. Sci., 24, 627-641.

10. _____, 1972: "Quasi-Geostrophic versus Non-geostrophic Frontogenesis." J. Atmos. Sci., 29, 3-10.

11. _____, 1973: Numerical Simulation of Steady-State Fronts. Unpublished Manuscript.

INITIAL DISTRIBUTION LIST

		No. Copies
1.	Defense Documentation Center Cameron Station Alexandria, Virginia 22314	2
2.	Library, Code 0212 Naval Postgraduate School Monterey, California 93940	2
3.	Dr. R. T. Williams, Code 51Wu Department of Meteorology Naval Postgraduate School Monterey, California 93940	10
4.	Commanding Officer Naval Weather Service Command Naval Weather Service Headquarters Washington Navy Yard Washington, D. C. 20390	1
5.	Officer in Charge Environmental Prediction Research Facility Naval Postgraduate School Monterey, California 93940	1
6.	Commanding Officer Fleet Numerical Weather Central Naval Postgraduate School Monterey, California 93940	1
7.	AFCRL - Research Library L. G. Hanscom Field Attn: Nancy Davis/Stop 29 Bedford, Massachusetts 01730	1
8.	Director, Naval Research Laboratory Attn: Tech. Services Information Officer Washington, D. C. 20390	1
9.	Department of Meteorology, Code 51 Naval Postgraduate School Monterey, California 93940	1
10.	Department of Oceanography, Code 58 Naval Postgraduate School Monterey, California 93940	1

11. Office of Naval Research — 1
Department of the Navy
Washington, D. C. 20360

12. Commander, Air Weather Service — 1
Military Airlift Command
United States Air Force
Scott Air Force Base, Illinois 62226

13. Dr. F. J. Winninghoff — 1
1085 Steeles Avenue, #503
Willowdale (Toronto), Ontario M2R2T1

14. Professor J. Bjerknes — 1
Department of Meteorology
UCLA
Los Angeles, California 90024

15. Atmospheric Sciences Library — 1
National Oceanic & Atmospheric Administration
Silver Spring, Maryland 20910

16. Professor Victor Starr — 1
Department of Meteorology
M.I.T.
Cambridge, Massachusetts 02139

17. Dr. J. Pedlosky — 1
Department of Geophysical Science
University of Chicago
Chicago, Illinois 60637

18. Dr. Joanne Simpson — 1
Experimental Meteorology Branch
National Oceanic & Atmospheric Administration
Coral Gables, Florida 33124

19. National Center for Atmospheric Research — 1
Box 1470
Boulder, Colorado 80302

20. Dr. Fred Shuman, Director — 1
National Meteorological Center
National Oceanic & Atmospheric Administration
Suitland, Maryland 20390

21. Dr. J. Smagorinsky, Director — 1
Geophysical Fluid Dynamics Laboratory
Princeton University
Princeton, New Jersey 08540

22. Professor N. A. Phillips — 1
Department of Meteorology
M.I.T.
Cambridge, Massachusetts 02139

23. Dr. B. J. Hoskins — 1
U.K. Universities Modeling Group
University of Reading
Reading, England

24. Professor J. Holmboe — 1
Department of Meteorology
UCLA
Los Angeles, California 90024

25. Professor J. G. Charney — 1
54-1424
M.I.T.
Cambridge, Massachusetts 02139

26. Dr. F. Sanders — 1
Department of Meteorology
M.I.T.
Cambridge, Massachusetts 02139

27. Professor K. Ooyama — 1
National Center for Atmospheric Research
Box 1470
Boulder, Colorado 80302

28. Dr. M. G. Wurtele — 1
Department of Meteorology
UCLA
Los Angeles, California 90024

29. Dr. A. Arakawa — 1
Department of Meteorology
UCLA
Los Angeles, California 90024

30. Dr. G. Haltiner, Chairman, Code 51Ha — 1
Department of Meteorology
Naval Postgraduate School
Monterey, California 93940

31. Dr. R. L. Haney, Code 51Hy — 1
Department of Meteorology
Naval Postgraduate School
Monterey, California 93940

32. Dr. R. Elsberry, Code 51Es — 1
Department of Meteorology
Naval Postgraduate School
Monterey, California 93940

33. Dr. C.-P. Chang, Code 51Cj — 1
Department of Meteorology
Naval Postgraduate School
Monterey, California 93940

34. Dr. R. Renard, Code 51Rd — 1
Department of Meteorology
Naval Postgraduate School
Monterey, California 93940

35. Dr. K. Davidson, Code 51Ds — 1
Department of Meteorology
Naval Postgraduate School
Monterey, California 93940

36. Dr. R. Alberty — 1
National Severe Storms Laboratory
1616 Halley Circle
Norman, Oklahoma 73069

37. Dr. Peter H. Stone — 1
Institute for Space Studies
2880 Broadway
New York, New York 10025

38. Dr. S. Piacsek, Code 7750 — 1
Naval Research Laboratory
Washington, D. C. 20390

39. Dr. E. N. Lorenz — 1
Department of Meteorology
M.I.T.
Cambridge, Massachusetts 02139

40. Dr. D. Houghton — 1
Department of Meteorology
University of Wisconsin
Madison, Wisconsin 53706

41. Dr. S. K. Kao — 1
Department of Meteorology
University of Utah
Salt Lake City, Utah 84112

42. Dr. A. P. Ingersoll — 1
Division of Geological and Planetary Sciences
California Institute of Technology
Pasadena, California 91101

43. Dr. J. Wallace 1
Department of Atmospheric Sciences
University of Washington
Seattle, Washington 98105

44. Dr. J. Holton 1
Department of Atmospheric Sciences
University of Washington
Seattle, Washington 98105

45. Dr. J. Young 1
Department of Meteorology
University of Wisconsin
Madison, Wisconsin 53706

46. Dr. T. Ogura 1
Laboratory for Atmospheric Research
University of Illinois
Urbana, Illinois 61801

47. Dr. Y. Sasaki 1
Department of Meteorology
University of Oklahoma
Norman, Oklahoma 73069

48. Dr. J. Mahlman 1
Geophysical Fluid Dynamics Laboratory
Princeton University
Princeton, New Jersey 08540

49. Dr. R. Alexander 1
The Rand Corporation
1700 Main Street
Santa Monica, California 90406

50. Dr. J. L. Lewis 1
Laboratory for Atmospheric Research
University of Illinois
Urbana, Illinois 61801

51. Dr. S. Mudrick 1
AFCRL (LYD)
L. G. Hanscom Field
Bedford, Massachusetts 01730

52. Dr. W. L. Gates 1
The Rand Corporation
1700 Main Street
Santa Monica, California 90406

53. Professor F. Bretherton 1
John Hopkins University
Baltimore, Maryland 21218

54. Lieutenant C. James Cornelius 1
716 Linden Avenue
Pine Beach, New Jersey 08741

55. Naval Oceanographic Office 1
Library (Code 3330)
Washington, D. C. 20373

SECURITY CLASSIFICATION OF THIS PAGE (When Date Entered)

REPORT DOCUMENTATION PAGE

READ INSTRUCTIONS BEFORE COMPLETING FORM

1. REPORT NUMBER

2. GOVT ACCESSION NO.

3. RECIPIENT'S CATALOG NUMBER

4. TITLE (and Subtitle)

The Inclusion of Moisture in a Numerical Model of Steady-State Fronts

5. TYPE OF REPORT & PERIOD COVERED
Master's Thesis
March 1974

6. PERFORMING ORG. REPORT NUMBER

7. AUTHOR(s)

Clifford James Cornelius, Jr.

8. CONTRACT OR GRANT NUMBER(s)

9. PERFORMING ORGANIZATION NAME AND ADDRESS

Naval Postgraduate School
Monterey, California 93940

10. PROGRAM ELEMENT, PROJECT, TASK AREA & WORK UNIT NUMBERS

11. CONTROLLING OFFICE NAME AND ADDRESS

Naval Postgraduate School
Monterey, California 93940

12. REPORT DATE
March 1974

13. NUMBER OF PAGES
80

14. MONITORING AGENCY NAME & ADDRESS(if different from Controlling Office)

Naval Postgraduate School
Monterey, California 93940

15. SECURITY CLASS. (of this report)
Unclassified

15a. DECLASSIFICATION/DOWNGRADING SCHEDULE

16. DISTRIBUTION STATEMENT (of this Report)

Approved for public release; distribution unlimited.

17. DISTRIBUTION STATEMENT (of the abstract entered in Block 20, if different from Report)

18. SUPPLEMENTARY NOTES

19. KEY WORDS (Continue on reverse side if necessary and identify by block number)

Frontogenesis
Moisture
Numerical integration

20. ABSTRACT (Continue on reverse side if necessary and identify by block number)

The numerical frontogenesis model of Williams (1973) is modified to include moisture with its subsequent condensation and release of latent heating. The turbulent diffusions of momentum, heat, and moisture are represented with various coefficients. The numerical solutions show realistic quasi-steady fronts forming within one or two days. These solutions are examined and compared over

DD FORM 1 JAN 73 1473 (Page 1)

EDITION OF 1 NOV 65 IS OBSOLETE
S/N 0102-014-6601

SECURITY CLASSIFICATION OF THIS PAGE (When Date Entered)

a range of the various coefficients, and various ranges of temperature.

Inclusion of moisture in the model causes intensification of baroclinicity at mid and upper levels. Also noted is a sensitivity of the moist model to reference potential temperature due to the exponential relationship between saturation vapor pressure and temperature.

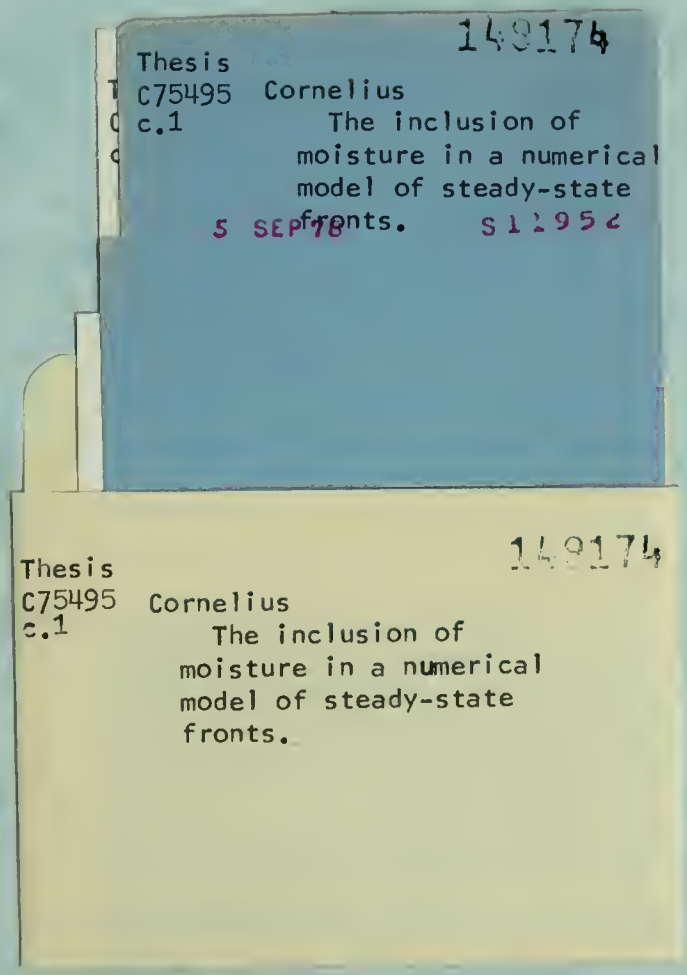

149174
Thesis
C75495 Cornelius
c.1 The inclusion of
moisture in a numerical
model of steady-state
fronts.